Electrochemically Induced Alkalinity Enhancement Increases Coral Growth Rates in the Local Microenvironment

Patrick M. Kiel
pkiel@earth.miami.edu
University of Miami

Matthew McConnell
Matthewm1818@gmail.com
University of Miami

Albert Boyd
albert.boyd@noaa.gov
Rosenstiel School of Marine, University of Miami

Nash Soderberg
nash.soderberg@noaa.gov
Rosenstiel School of Marine, University of Miami

Prannoy Suraneni
suranenip@miami.edu
University of Miami

Vivek N. Prakash
vprakash@miami.edu
University of Miami

Ian C. Enochs
ian.enochs@noaa.gov
NOAA

Research Article

Keywords: coral restoration, alkalinity enhancement, coral growth, geochemical engineering

DOI: https://doi.org/

Additional Declarations: No competing interests reported.

Article Title

Electrochemically Induced Alkalinity Enhancement Increases Coral Growth Rates in the Local Microenvironment

Authors

Patrick M. Kiel[1,2,3*], Matthew McConnell[1], Albert Boyd[2,3], Nash Soderberg[2,3], Prannoy Suraneni[4], Vivek N. Prakash[1,5,6], and Ian C. Enochs[3]

Affiliations

1. Department of Marine Biology and Ecology, Rosenstiel School of Marine, Atmospheric and Earth Science, University of Miami, Miami, Florida, USA.
2. Cooperative Institute for Marine and Atmospheric Studies, Rosenstiel School of Marine, Atmospheric and Earth Science, University of Miami, Miami, Florida, USA.
3. Atlantic Oceanographic and Meteorological Laboratory, Ocean Chemistry and Ecosystem Division, NOAA, Miami, Florida, USA.
4. Civil and Architectural Engineering, College of Engineering, University of Miami, Coral Gables, Florida, USA.
5. Department of Physics, College of Arts & Sciences, University of Miami, Coral Gables, Florida, USA.
6. Department of Biology, College of Arts & Sciences, University of Miami, Coral Gables, Florida, USA.

Corresponding author

pkiel@earth.miami.edu

ORCIDs

- P.M.K.: 0000-0002-5743-3128
- M.M.: 0009-0008-5508-0403
- A.B.: 0009-0007-9657-3135
- N.S.: 0000-0002-3155-4167
- P.S.: 0000-0002-0899-2601
- V.N.P.: 0000-0003-4569-6462
- I.C.E.: 0000-0002-8867-0361

Abstract

Coral reef ecosystem health is rapidly declining worldwide. Restoration strategies such as propagation and outplanting aim to recover reef function but can be hindered by slow growth rates that limit scalability, necessitating technologies that accelerate growth to match the scale of reef degradation. Electrochemically induced alkalinity enhancement (eAE) offers a promising approach to locally enhance carbonate chemistry and favor calcification. We developed replicate eAE systems composed of steel cathodes and a platinized anode housed within an evacuation pump to remove oxidative waste products. System performance was evaluated with carbonate chemistry incubations, microelectrode profiling, and two laboratory experiments with *Acropora cervicornis* and *Pseudodiploria clivosa* microfragments. The eAE system created a high alkalinity microenvironment under 1 cm s^{-1} flow speeds, elevating pH_T by 0.14 ± 0.02 to 8.16 at the height of the 'short' 5 mm *P. clivosa* microfragments. At 3 cm s^{-1}, pH_T at 5 mm was 8.03, and under both flow speeds, pH_T returned to bulk levels (8.02) at the height of the 15 mm *P. clivosa* and 50 mm *A. cervicornis* fragments. After sixty days, short *P. clivosa* microfragments exposed to eAE calcified 43% faster and had 53% greater planar tissue growth rates than controls. These enhancements occurred exclusively within the elevated pH boundary layer and did not extend to taller fragments (≥15 mm), highlighting eAE's limited spatial extent. Our findings demonstrate eAE's potential to accelerate microfragment skirting rates. Integrating eAE into coral propagation pipelines could enhance nursery productivity, reduce generation times, and improve the overall scalability of reef restoration efforts.

Keywords: coral restoration, alkalinity enhancement, coral growth, geochemical engineering

Statements and Declarations

Conflicts of Interest

The authors declare no competing interests.

Funding

This material is based upon work supported by the National Science Foundation Graduate Research Fellowship Program, Grant No. 1938060, awarded to P.M.K. Additional funding was provided by the University of Miami's Laboratory for Integrative Knowledge (ULINK: Engineering Corals for Climate Change Resilience) awarded to P.S., V.N.P., I.C.E., University of Miami start-up funding to V.N.P., and National Oceanographic and Atmospheric Administration Coral Reef Conservation Program to I.C.E. Any opinions, findings, conclusions or recommendations expressed in this material are those of the authors and do not necessarily reflect the views of

the National Science Foundation or the National Oceanographic and Atmospheric Administration.

Acknowledgements

The authors thank Diego Lirman for providing corals and resources for this project, Mark Capron for helpful discussions during the project's inception, and Brian Haus for providing laboratory facilities in the Alfred C. Glassell, Jr. SUSTAIN Laboratory. We also acknowledge members of the Suraneni and Prakash Labs, as well as the NOAA AOML Coral Program, for useful discussions.

Introduction

Coral reefs rely on a robust, three-dimensional structure to sustain the highest marine species concentrations, collectively generating and protecting billions of USD in value for the global economy (Graham and Nash 2013; Torres-Pulliza et al. 2020). Unfortunately, the rapid decline in carbonate production driven by the compounding effects of local and global stressors has eroded reef structural complexity and limited their ecosystem services (Alvarez-Filip et al. 2009; Perry et al. 2013).

To combat these challenges, resource managers have developed active restoration programs that propagate and outplant corals back onto the reef (Young et al. 2012; Boström-Einarsson et al. 2020). These efforts are increasingly acknowledged as essential to ensure coral reef persistence in an era marked by rapid global change (Kleypas et al. 2021; Webb et al. 2023). However, the current scale of these operations and their output is insufficient to meet the magnitude of the stressors acting upon them or the spatial extent of the degradation. Therefore, in addition to stressor mitigation, effective strategies must be implemented throughout the restoration pipeline to conserve ecosystem services.

Slow growth rates inherently constrain coral restoration operations, but targeted interventions offer opportunities to optimize and accelerate growth. To this end, the restoration community has increasingly adopted the microfragmentation method that involves cutting large mounding corals into multiple small pieces less than 10 cm^2 (Forsman et al. 2015). Practitioners cultivate fragments in nurseries before returning the corals to the reef, where tenfold increases in planar tissue growth rates compared to larger fragments can be achieved (Page et al. 2018).

An alternative approach to increase growth rates is alkalinity enhancement (AE). AE with carbonate or bicarbonate mineral addition has been shown to increase growth rates between twofold and tenfold and increase the survivorship of coral recruits (Marubini and Thake 1999; Langdon et al. 2000; Herfort et al. 2008; Ruszczyk et al. 2025). However, these successes were limited to closed, experimental systems with relatively small volumes, and an AE trial on a reef flat resulted in increases in growth rates two orders of magnitude lower than those observed in laboratory studies (Albright et al. 2016). Alternatively, seawater electrolysis can directly increase alkalinity (Willauer et al. 2014; Eisaman et al. 2023). Electrochemically induced alkalinity enhancement (eAE) may be favored because it selectively modifies alkalinity in a small volume of seawater directly surrounding the corals, rather than requiring alteration of the bulk seawater (Hilbertz and Goreau 1996).

Throughout its four-decade history, there has been encouraging evidence that eAE improves coral growth rates (Goreau 2013, 2022). Small-scale field deployments have observed a wide range of growth rate enhancements from approximately 30% to tenfold, and similar enhancements have been observed

in limited laboratory studies (Sabater and Yap 2002; Strömberg et al. 2010; Huang et al. 2020; Goreau 2022; Samidon et al. 2022).

However, multiple eAE studies have observed no increases in growth rates and documented declines in survivorship and coral health (Borell et al. 2010; Romatzki 2014; Chavanich et al. 2015). Confounding results may be attributed to environmental factors such as flow, or species-specific or morphological differences, where only certain size classes or coral shapes experience enhanced growth. Moreover, the region of AE may be spatially limited to regions most proximal to the cathode where the alkalinity is leached (Sabater and Yap 2002; Samidon et al. 2022). Finally, there is concern that the growth enhancements are non-linear such that the corals initially experience rapid increases in growth during the first three to six months, followed by growth rates coalescing with controls (Sabater and Yap 2004; Huang et al. 2020). Ultimately, these concerns, coupled with the cross-disciplinary challenges, have limited further exploration of the technology and widespread adoption within the restoration community (Boström-Einarsson et al. 2020).

Therefore, this study aims to identify the mechanisms constraining eAE and investigate whether eAE develops an enhanced microenvironment that the restoration community can reliably leverage. To test the effect of eAE on coral propagation, we used pH microsensors and incubations to measure eAE altered carbonate chemistry, and we conducted two coral growth experiments with *Acropora cervicornis* and *Pseudodiploria clivosa*.

Methods

eAE System Construction

Four identical eAE systems were constructed in flow-through aquariums. Cathodes were prepared by trimming, etching, and cleaning 2.5 cm steel weld studs (~20 cm^2 surface area; 93865A540, McMaster-Carr). Identically sized acrylic pucks were used as inert controls. The anode consisted of a 7.5 cm by 15.0 cm titanium mesh with a 0.5 µm platinum layer fashioned into a cylinder with a diameter of 5 cm (TI-M-01-ME.PTC, American Elements), providing an estimated surface area of 1,500 cm^2, sufficiently larger than the total surface area of the cathodes (i.e., > 5:1) to prevent the anodic reactions from limiting the cathodic reactions (Bard and Faulkner 2001). Electrodes were fixed to PVC-jacketed copper wire, and all connections were sealed with an epoxy coating. The anode was housed in a 5 cm PVC pipe, which was connected to a brushless peristaltic pump (A200BX, Anko) designed to evacuate chlorine and acidity generated at the anode. Cathodes and inert substrates were arranged in a circular pattern around the anode pump (Figure 1; Figure S1) and connected in series to a power supply (MX100QP, Aim-TTi) regulated by a custom LabView script (National Instruments) to control and log power output.

eAE System Performance

Impact of eAE on seawater carbonate chemistry

Seawater incubations were conducted to estimate the changes in carbonate chemistry above the eAE cathodes as a function of electrical current density (0.5, 1, and 3 A/m^2), as well as above an inert acrylic puck serving as the control condition that was not connected to the circuit. A scaled-down eAE system with a single cathode was prepared in a closed 4 L polypropylene container. The anode pump did not evacuate seawater for these experiments to maintain a constant water volume. A recirculating pump (Nano 565, Koralia) provided constant water flow in the incubation chamber throughout the three-hour incubation. Three incubations per electrical current density and control conditions were performed for a total of 12 incubations. For each incubation, the chamber was filled with 1 µm filtered seawater collected from Bear Cut, Miami, Florida. Water samples (500 mL) were collected before and after the incubations and fixed with the addition of 200 µL mercuric chloride. Samples were analyzed for the complete determination of the carbonate chemistry system including pH (8454 UV–Vis Spectrophotometer, Agilent Cary), total alkalinity (A_T; 855 Robotic Titrosampler, Metrohm), dissolved inorganic carbon (DIC; AS-C3, Apollo SciTech), and salinity (DMA 5000 M, Anton Paar). Additional 40 mL water samples were collected, filtered through 0.45 µm syringe filters, and immediately frozen for analysis of nutrients (nitrate, nitrite, phosphate and ammonium; AutoAnalyzer3, SEAL). Nutrient concentrations were minimal and were used to adjust the contribution of organic alkalinity prior to calculating the carbonate chemistry system with the seacarb library (Gattuso et al. 2024) in the R environment to determine the pCO_2 and the aragonite saturation state (Ω_{Ar}). Changes in carbonate chemistry from final and initial samples were standardized by the incubation time and were blank-corrected from the control incubations to account for non-eAE induced changes in carbonate chemistry due to microbial activity and/or evaporation (Smith and Kinsey 1978; Schoepf et al. 2017).

Impact of flow speeds and electrical current density on the pH boundary layer

The pH boundary layer above the cathode was quantified as a function of water flow and electrical current density using the single cathode setup, which was housed in an open-top, flow-through flume. The flume was chosen to prevent the buildup of an upstream concentration gradient. Volumetric flows through the working section of the flume were calibrated with particle image velocimetry to determine the bulk flow mean velocities, hereinafter referred to as flow speeds, and were set to 0, 1, and 3 cm s^{-1}, equating to a volumetric flow rate of 0, 2.3, and 6.4 L min^{-1} (Ruszczyk et al. 2024). These three flow speeds were chosen to produce the thickest possible boundary layers, the boundary layers expected during the growth experiments, and the boundary layers expected at a local coral nursery based on the average flow

speeds on a reef approximately 1 km from the University of Miami Coral Nursery (Enochs et al. 2023). For each investigation, the cathode or inert puck was placed in the center of the flume and the anode was positioned 15 cm downstream. The anode pump did not evacuate seawater to maintain steady flow conditions across the tested conditions. The flume and eAE system were operated at set flow speed and electrical current density for two hours prior to profiling to allow steady-state pH conditions to develop.

pH profiles were measured with a microprofiling system equipped with a pH microelectrode (pH-50, Unisense), calibrated daily with NBS buffers. Values of NBS-scale pH (pH_{NBS}) were converted to total scale (pH_T) using seacarb. The microelectrode tip was initially positioned at the cathode surface with the aid of a camera (Imager CX2, LaVision) and moved vertically upward into the water column with a micromanipulator (MM33-2, Unisense). The pH was measured at 37 steps spanning 2.5 cm for each profile, and the average of 10 measurements in 30 seconds was taken as the individual step's pH (Supplementary Methods). Profiles were initially standardized by converting pH_T into $[H^+]$ and dividing the $[H^+]$ of each step by the bulk $[H^+]$ of its respective profile. To account for minor variations among replicate profiles, each standardized profile was then multiplied by the average bulk $[H^+]$ across all profiles and converted back into pH_T. These standardized pH profiles were used in all subsequent analyses (Schoepf et al. 2018). Hyperbolic tangent models were fit to the profiles, and the pH boundary layer heights were estimated from the models (Nishihara and Ackerman 2007).

pH profiles were collected to investigate the impact of flow speed and current density on pH boundary layer height above the cathode using the previously described methods. To investigate the impact of flow speed on pH boundary layer height above the cathode, three replicate pH profiles were collected at flow speeds of 0, 1, and 3 cm s^{-1} using a fixed electrical current density of 1 A m^{-2}. To investigate the impact of electrical current density on pH boundary layer height above the cathode, three replicate pH profiles were collected at electrical current densities of 0.5, 1, and 3 A m^{-2}, as well as above an inert acrylic puck, at a constant flow speed of 1 cm s^{-1}.

eAE Impact on Coral Growth

Impact of eAE on Acropora cervicornis

To investigate the impact of eAE on the growth and fitness of a species frequently used in Atlantic coral propagation and restoration, eight fragments from seven genets (56 fragments) were collected from the University of Miami Coral Nursery (25.6763°N 80.0987°W, 8 m depth). Fragments were trimmed to five centimeters with a single apical tip, and two replicates per genet were randomly distributed to four separate aquariums. Fragments were then affixed to either a cathode or an inert acrylic puck with cyanoacrylate glue (Coral Glue Gel, Bulk Reef Supply). Thus, each aquarium held an eAE and control fragment from each genet with replication across

four aquariums. Additionally, each aquarium contained three blank cathodes, referred hereinafter as bare eAE substrates, that were partially covered with cyanoacrylate glue to simulate the surface area covered by a coral and estimate total abiotic precipitation. Corals were allowed to heal and acclimate to the aquarium for one week prior to initiating the experiment.

Following the acclimation period, the eAE system was set to maintain a current density 1 A m^{-2}. The cathodic reduction potential was measured at -1.15 V/AgCl, placing the system in the water reduction domain (Carré et al. 2020). Treatment conditions were maintained for 60 days (October to December 2023). Throughout, aquaria were maintained following Enochs *et al.* (2018). Briefly, fresh seawater from Biscayne Bay was UV-sterilized, filtered, and flowed into independent 150 L aquariums through weekly-calibrated needle valves at 700 mL min^{-1}, resulting in a turnover every 3.6 h. The anode pump evacuated water at 300 mL min^{-1}, with daily calibration. Temperature (27° C) was monitored (TTD25C, ProSense) and controlled with a 300 W heater (TH300, Finnex) and a titanium chiller coil (Hotspot Energy). Light was provided by LED arrays (Radion XR30 G6 PRO, EcoTech Marine), set with a three-hour dawn and dusk ramp and a six-hour, static mid-day light level as measured at the coral surface (250 µmol m^{-2} s^{-1}; MQ-510, Apogee). Bulk pH in the tank was monitored continuously with a Durafet pH electrode (Honeywell), and discrete water samples were collected twice weekly to calibrate pH probes and determine the carbonate chemistry system including pH, TA, DIC, salinity, pCO_2, and Ω_{Ar} as described previously. Corals were target fed 5 mL of a 3.3g L^{-1} concentrated slurry (Reef-Roids, Polyp Labs) two times per week.

Coral and cathode mass was measured using the buoyant weight technique (Jokiel et al. 1978), using a calibrated analytical balance (Pioneer 0.0001 g precision, Ohaus) every two weeks. Corals were suspended from tungsten wire (0.05 mm) in a temperature-controlled (27° C) seawater bath. Temperature and salinity were recorded during each mass measurement with a conductivity meter (EcoSense EC300A, YSI) and converted into density with the seacarb package. Calcification was calculated as the difference in the weekly mass and was standardized to colony surface area as determined from 3D scanning (HDI Advance R2, 3D3 Solutions) at the beginning of the experiment following the methods of Enochs *et al.* (2014). For corals grown on eAE substrates, an adjusted calcification rate was calculated by subtracting the contribution of abiotic mineral precipitation as determined from the mean growth rate of the bare eAE substrates. Coral health and survival were assessed visually by monitoring polyp expansion and discoloration.

Impact of eAE on Pseudodiploria clivosa fragments with different heights

A second experiment was conducted to test whether eAE influenced the brain coral *P. clivosa* microfragments' growth rate and whether distance from the cathode (fragment height) influenced growth rates. Eight *P. clivosa*

fragments from six genets (48 fragments) were collected from the University of Miami Coral Nursery. Fragments were trimmed into 2.25 cm^2 squares with a diamond-bit band saw (C-40, Gryphon). The heights of the corals were trimmed by removing part of the skeleton below the tissue layer, and the fragments were evenly divided into short (5 mm) and tall (15 mm) fragment height groups (Figure 1). The heights were chosen to, respectively, place the corals inside and outside of the pH boundary layer. Four aquariums were assigned as either eAE or control, and the corals were randomly distributed across the aquariums. Thus, each aquarium held a tall and short fragment from each genet. Corals in eAE aquariums were affixed to the steel cathodes, and corals in the control aquariums were affixed to the inert acrylic pucks. Additionally, the two eAE aquariums received three blank cathodes that were partially covered with cyanoacrylate glue to simulate the surface area covered by a coral and estimate total abiotic precipitation. Corals were allowed to heal and acclimate to the aquarium for one week prior to initiating the experiment.

Following the acclimation period, electrochemical conditions in the eAE aquaria were set to match those of the *A. cervicornis* experiment. Treatment conditions were maintained for 60 days from February to April 2024. During this period, corals were maintained in polycarbonate aquaria (50 L; Cambro), which were housed within two larger fiberglass water baths, each containing one eAE aquarium and one control aquarium. Each aquarium was equipped and programmed identically to the previous experiment, including a circulation pump, aquarium heater, temperature recorder, and LED array. Continuous pH monitoring was not performed in this experiment, as no measurable bulk pH change had been observed in the initial study. Weekly water samples, however, were collected to characterize the complete carbonate chemistry system, including pH, using methods consistent with the previous growth experiment. Aquaria were continuously flushed with fresh filtered seawater at a rate of 500 mL min^{-1}, resulting in a complete turnover every 2 hours. Anode chambers were evacuated at 300 mL min^{-1}, with flow rates calibrated daily. Corals were individually target-fed twice weekly with 5 mL of the 3.3g L^{-1} concentrated slurry (Reef-Roids, Polyp Labs).

Gross calcification rates were measured using methods identical to those of the *A. cervicornis* experiment. For this experiment, the eAE substrates received additional cleaning on the underside of the cathodes at the ring terminal junction with a wire brush to ensure electrical continuity. Consequently, reported abiotic mineral precipitation rates are likely underestimates, but cleaning regimens were uniform within each experiment for both bare eAE and coral eAE substrates. To assess growth independent of abiotic precipitation, planar images were collected in a camera rig that consistently maintained the corals at a fixed distance from the camera (DeMerlis et al. 2022). The images were calibrated with Fiji (Schindelin et al. 2012), and the planar areas covered by live tissue were recorded. Planar tissue growth rates were estimated from slopes calculated by the estimated marginal means of repeated measures mixed-effects models. Image analysis

error analysis was estimated by measuring the fixed diameter of the substrates in all photos and was deemed consistent and negligible.

At the conclusion of the experiment, the dark-adapted yield of photosystem II (Fv/Fm) was measured for all corals to determine if eAE induced measurable changes in coral photophysiology. To measure Fv/Fm, corals were first dark-acclimated for 30 min following the conclusion of the programmed sunset and then measured using an imaging pulse amplitude-modulated fluorometer (Imaging-PAM MAXI Version, Walz, Germany). A circular region of interest was digitally centered on each coral fragment, and the software settings were set following Palacio-Castro *et al.* (2022): measuring light intensity = 1; measuring light frequency = 1; dampening = 2; saturating pulse intensity = 7; and saturating pulse width = 4. Gain was manually adjusted to elicit an FT measurement above the 0.12 threshold.

Statistics and Data Analysis

All statistical analyses were performed in the R environment (v 4.4.1, R Core Team 2024). Model residuals were assessed for normality and homogeneity of variance both visually and with formal tests including Shapiro-Wilk tests for normality and Levene's test for homoscedasticity. When assumptions were met, one-way ANOVAs were used, followed by Tukey's post-hoc tests for multiple pairwise comparisons. In cases where assumptions were violated or the design included repeated measures or nesting structure of aquarium replicates, linear mixed-effects models (LMMs) or generalized linear mixed-effects models (GLMMs) were fit as appropriate. LMMs were fit using the lmer function and GLMMs were fit using the glmer function from the lme4 package. For LMMs, Satterthwaite's approximation was used to estimate degrees of freedom via the lmerTest package, and Type III ANOVAs were performed. For GLMMs, models were fit with log-link functions and Wald *t*-tests assuming infinite degrees of freedom were reported. For repeated measures data including coral masses and planar areas, the coral ID was included as an additional random effect. Post hoc comparisons of estimated marginal means (EMMs) were conducted using the emmeans package with Tukey adjustment for multiple comparisons for all mixed effects models. In the analysis of planar areas over time, rates were estimated as slopes using emtrends, and percent differences between treatment groups were calculated from these slope estimates. Statistical significance for all models was evaluated at $\alpha = 0.05$ with adjustments for multiple comparisons as appropriate.

Results

eAE System Performance

Impact of eAE on seawater carbonate chemistry

Closed-system incubations revealed a significant effect of electrical current density on the net decrease in A_T during the three-hour incubation period (ANOVA $F(2, 6) = 51.94$, $p < 0.001$). Alkalinity decreased significantly faster at the highest electrical current density of 3 A m^{-2} (-162 ± 22 µmol kg^{-1} h^{-1}; ±1 SD) compared to both 1 A m^{-2} (-38 ± 14 µmol kg^{-1} h^{-1}; Tukey's HSD, $p < 0.001$) and 0.5 A m^{-2} (-15 ± 21 µmol kg^{-1} h^{-1}; $p < 0.001$), while no significant difference was observed between the two lower electrical current densities (Figure S4). In contrast, there were no significant differences in DIC changes among the three treatments: 3 A m^{-2} (-24 ± 8 µmol kg^{-1} h^{-1}), 1 A m^{-2} (-7 ± 6 µmol kg^{-1} h^{-1}) and 0.5 A m^{-2} (-9 ± 12 µmol kg^{-1} h^{-1}). Consequently, there were significant differences observed in the calculated changes of pCO2, $[CO_2]$, $[HCO_3^-]$, and $[CO_3^{2-}]$ across treatments during the incubations (Table S1).

Impact of water flow and electrical current density on the pH boundary layer

pH microprofiles above the cathodes revealed a locally enhanced microenvironment, the thickness and magnitude of which were modulated by electrical current density and flow speed (Table S2). Across all profiles, the pH_T was greater than 8.70 at the cathode-seawater interface (height = 0 mm) and attenuated to 8.02 in the bulk water (height = 25 mm).

Under constant electrical current density (1 A m^{-2}) and varying flow speeds, the pH_T at the cathode-seawater interface was consistently elevated (8.87 ± 0.02) compared to the bulk water and was indistinguishable between profiles (Figure 2). The pH boundary layer height decreased significantly with increasing flow speed (ANOVA $F(2, 6) = 100.5$, $p < 0.0001$), with the pH boundary layer significantly thicker at 0 cm s^{-1} (21.34 ± 0.08 mm) compared to both 1 cm s^{-1} (15.05 ± 1.82 mm; $p <0.01$) and 3 cm s^{-1} (5.92 ± 1.44 mm; $p < 0.0001$). All pairwise comparisons of pH boundary layer heights among flow speeds were statistically significant (Table S3). Additionally, significant differences in pH_T were observed at 5 mm above the cathode (ANOVA $F(2, 6) = 100.9$, $p < 0.0001$). At this height, pH_T was significantly higher at a flow speed of 0 cm s^{-1} (8.22 ± 0.01) compared to both 1 cm s^{-1} (8.16 ± 0.02; $p < 0.05$) and 3 cm s^{-1} (8.03 ± 0.01; $p < 0.0001$). At 15 mm, pH_T differences remained significant (ANOVA $F(2, 6) = 358.3$, $p <0.00001$), but only the 0 cm s^{-1} (8.05 ± 0.00; $p < 0.00001$) remained elevated relative to the bulk flow, while both 1 cm s^{-1} and 3 cm s^{-1} conditions merged with bulk values (Table S2). There were no significant differences observed in the pH_T at 0 mm above the cathode.

Under constant flow speed (1 cm s^{-1}) and varying electrical current densities, the pH_T at the cathode-seawater interface was consistently elevated relative to the bulk water and differed significantly among treatments (ANOVA $F(2, 6) = 60.0$, $p < 0.001$). Interface pH_T was lowest at 0.5 A m^{-2} (8.69 ± 0.04), significantly increasing at 1.0 A m^{-2} (8.87 ± 0.02; $p < 0.01$), and 3.0 A m^{-2} (9.02 ± 0.05; $p < 0.0001$), with all pairwise comparisons between electrical current densities being statistically significant (Figure

S5). Boundary layer height also increased significantly with increasing electrical current density (ANOVA $F(2, 6) = 145.6$, $p < 0.0001$). The thinnest pH boundary layer was observed at 0.5 A m^{-2} (10.31 ± 0.82 mm), compared to significantly thicker pH boundary layers at 1.0 A m^{-2} (14.64 ± 0.85 mm; $p < 0.01$) and 3.0 A m^{-2} (21.19 ± 0.68 mm; $p < 0.00001$). All pairwise differences in pH boundary layer heights among electrical current densities were statistically significant (Table S3). At 5 mm above the cathode, pH_T varied significantly with electrical current density (ANOVA $F(2, 6) = 50.8$, $p < 0.001$). pH_T at 0.5 A m^{-2} (8.06 ± 0.01) was significantly lower than at 1.0 A m^{-2} (8.15 ± 0.02; $p < 0.001$) and 3.0 A m^{-2} (8.19 ± 0.01; $p < 0.001$), though there was no significant difference between the latter two ($p > 0.05$). At 15 mm above the cathodes, pH_T differences remained significant among the electrical current densities (ANOVA $F(2, 6) = 139.2$, $p < 0.00001$), but only the 3 A m^{-2} treatment (8.04 ± 0.00; $p < 0.0001$) remained elevated relative to the bulk flow. The 0.5 A m^{-2} and 1.0 A m^{-2} treatments had pH_T values indistinguishable from bulk values (Table S2). In contrast, all profiles measured above inert acrylic pucks showed no pH_T elevation and, consequently, no detectable pH boundary layer (Figure S5).

The pH boundary layer heights during both growth experiments most closely resembled those observed at a flow speed of 1 cm s^{-1} and an electrical current density of 1 A m^{-2}, where the pH_T was 8.16 ± 0.02 at 5 mm and 8.02 ± 0.00 at 15 mm above the cathode (Table S2).

eAE Impact on Coral Growth

Impact of eAE on Acropora cervicornis

Bulk water carbonate chemistry (Table 1) did not differ significantly among aquarium replicates within the *A. cervicornis* experiment. The water chemistry was stable throughout the experiment except for a decrease in A_T and salinity over the course of November, which is likely attributed to unseasonably high rainfall in Miami (total: 23.8 cm; climatological anomaly: 14.8 cm; NOAA 2024).

All *A. cervicornis* fragments survived the 60-day experiment, and there were no signs of declining health in any of the corals. Corals grown on the inert acrylic pucks grew at an average rate of 6.70 ± 4.47 mg d^{-1}, granting an average area-standardized daily calcification rate of 0.37 ± 0.26 mg cm^{-2} d^{-1} (Figure 3). The bare eAE substrates had an abiotic precipitation rate of 34.05 ± 6.69 mg d^{-1}. Corals on the eAE substrates grew at an average rate of 41.45 ± 3.96 mg d^{-1}. After subtracting the average abiotic precipitation rates of the bare eAE substrates from the eAE corals, the average adjusted eAE coral growth rate was 7.95 ± 3.37 mg d^{-1}, and the adjusted average daily calcification rate was 0.45 ± 0.21 mg cm^{-2} d^{-1}. There were no significant differences between the adjusted eAE coral calcification rate and the inert control coral calcification rate ($p > 0.05$; Table S4), indicating all elevated mass changes on the eAE corals were from abiotic precipitation (Figure 3).

Further, there were no significant differences in growth rates among genets or among replicate aquaria ($p > 0.05$).

Impact of eAE on Pseudodiploria clivosa fragments with different heights

Bulk water carbonate chemistry (Table 1) did not differ significantly among aquarium replicates or treatments within the *P. clivosa* experiment. Across the two experiments, however, there was a significant overall difference in the carbonate chemistry system ($t = 12.365$; $p < 0.0001$; Table S5). Post-hoc pairwise comparisons revealed that $[CO_2]$ ($t = 12.365$; $p < 0.001$) and pCO_2 (12.852; $p < 0.001$) were significantly higher in the *A. cervicornis* experiment, while $[CO_3^{2-}]$ ($t = 8.772$; $p < 0.0001$) and Ω_{Ar} ($t = 9.093$; $p < 0.00001$) were significantly lower in the *A. cervicornis* experiment compared to the *P. clivosa* experiment (Table 1). Despite these bulk water differences, all measured carbonate chemistry values fell within normal ranges for Bear Cut, Miami, Florida, and may reflect seasonal variability in Biscayne Bay seawater (Enochs et al. 2019).

Short corals grown on the inert acrylic pucks grew at an average rate of 3.11 ± 1.18 mg d^{-1}, corresponding to a daily calcification rate of 0.38 ± 0.16 mg cm^{-2} d^{-1} when standardized to each coral's surface area (Figure 4). Tall corals grown on the inert acrylic pucks grew at a similar rate, averaging 3.19 ± 1.21 mg d^{-1}, with a corresponding daily calcification rate of 0.40 ± 0.15 mg cm^{-2} d^{-1}. The bare eAE substrates had an abiotic precipitation rate of 24.94 ± 3.69 mg d^{-1}. Short corals on the eAE substrates grew at an average rate of 29.79 ± 1.84 mg d^{-1}, and tall corals on the eAE substrates grew at an average rate of 28.28 ± 1.24 mg d^{-1}. After subtracting the abiotic precipitation rates of the bare eAE substrates from the eAE corals, the adjusted growth rate of tall eAE corals was 3.34 ± 1.24 mg d^{-1}, yielding a daily calcification rate of 0.42 ± 0.16 mg cm^{-2} d^{-1} (Figure 4). For the short eAE corals, the adjusted growth rate was 4.85 ± 1.84 mg d^{-1}, with a daily calcification rate of 0.60 ± 0.22 mg cm^{-2} d^{-1}.

There were significant effects of substrate type ($t(5.0) = 5.020$; $p < 0.001$), coral height ($t(42.3) = 4.738$; $p < 0.00001$), and their interaction ($t(42.0) = 3.740$; $p < 0.0001$; Table S6) on the daily calcification rates of the *P. clivosa* microfragments (Figure 4). Post-hoc pairwise comparisons revealed that only the short eAE corals calcified at significantly higher rates than all other treatment groups. Short eAE corals grew on average faster than the short corals on inert pucks ($t(4.962) = 5.020$; $p < 0.05$), the tall eAE corals ($t(42.272) = 4.737$; $p < 0.001$), and the tall corals on inert pucks ($t(4.962) = 4.558$; $p < 0.05$). This represents a 43% increase in daily calcification rates among the eAE corals grown within the pH boundary layer. There were no significant differences in growth rates among genets or among replicate aquaria ($p > 0.05$).

Abiotic precipitation rates on eAE bare cathodes did not differ significantly between the two growth experiments (Table S7), although the lower precipitation rate observed during the *P. clivosa* experiment (24.94 ±

3.69 mg d^{-1}) compared to the *A. cervicornis* experiment (34.05 ± 6.69 mg d^{-1}) likely reflects the additional cathode cleaning introduced in the *P. clivosa* experiment (Methods).

Enhanced areal growth rates in the short eAE corals were observed independently of abiotic mineral precipitation. There were significant effects of substrate ($t(136.4) = 4.500$; $p < 0.0001$), height ($t(136.7) = 5.447$; $p < 0.0001$), and their interaction ($t(136.4) = 2.976$; $p < 0.0001$) on the planar tissue growth rates of *P. clivosa* microfragments (Figure 5; Table S8). Post-hoc analysis revealed that only the short eAE corals (0.032 ± 0.020 cm^2 day^{-1}) had significantly higher planar tissue growth rates compared to the short corals on inert pucks (0.021 ± 0.020 cm^2 day^{-1}), representing a 52% increase in planar tissue growth rates ($t(137) = 4.499$, $p < 0.0001$). In contrast, the growth rates of tall eAE corals (0.019 ± 0.020 cm^2 day^{-1}) and tall corals on inert pucks (0.018 ± 0.020 cm^2 day^{-1}) were not significantly different ($p > 0.05$). Additionally, there were no significant differences in growth rates among genets or among replicate aquaria ($p > 0.05$).

At the conclusion of the experiment, there were no significant differences in measured photochemical efficiency values (Fv/Fm) between the eAE and inert corals or between the short and tall corals ($p > 0.05$; Table S9). Further, all corals survived the 60-day experiment, and there was no observable change in polyp expansion. There was, however, a significant effect of genet (ANOVA $F(5, 42) = 4.816$; $p < 0.01$; Table S10) on measured Fv/Fm, with genet 8 (Fv/Fm = 0.523 ± 0.0680) being significantly less photochemically efficient than genets 9 (Fv/Fm = 0.572 ± 0.0680; $p < 0.05$), A (Fv/Fm = 0.588 ± 0.0680; $p < 0.001$), and B (Fv/Fm = 0.574 ± 0.0680; $p < 0.05$; Figure S6).

Discussion

Our experiments demonstrated that eAE can significantly increase the growth of small coral fragments that reside fully within the elevated alkalinity microenvironment. Short *P. clivosa* microfragments (5 mm height) grown on eAE substrates exhibited markedly higher calcification and planar tissue growth rates than identical fragments on inert controls or taller fragments (15 mm height) grown on eAE substrates. After sixty days, *P. clivosa* microfragments grown on eAE substrates showed a roughly 43% higher daily calcification rate and a 52% greater planar tissue growth rate compared to conspecifics on inert acrylic pucks (Figure 4; Figure 5). These enhancements occurred only for the small corals that remained within the microenvironment of elevated pH immediately above the cathode, consistent with the microsensor measurements of pH elevated by an average of 0.14 units 5 mm above the cathode (Table S2). This finding supports prior field-based observations and provides empirical evidence in favor of the hypothesis proposed by Hilbertz and Goreau (1996) that eAE creates an enhanced pH microenvironment capable of increasing coral growth rates.

The growth responses we observed align with prior studies of eAE and alkalinity addition, while highlighting important differences in growth

metrics. Sabater and Yap (2002) similarly reported 50% faster skeletal thickening (girth growth) in *Porites cylindrica* branches closest to an eAE cathode, even though vertical extension rates did not increase. Likewise, a recent study by Samidon *et al.* (2022) found 30% greater planar tissue growth in a branching coral directly attached to an eAE substrate, but no effect on a massive coral where an epoxy layer separated the coral from the cathode. These field studies mirror our findings that only coral tissue within the enhanced pH boundary layer is stimulated to grow faster.

Notably, the growth enhancement we measured is modest compared to some anecdotal field reports of eAE. For example, Goreau *et al.* (2022) highlighted case studies that achieved two to ten-fold increases in linear extension of corals under long-term eAE treatment. It is likely that such dramatic case studies reflect confounding environmental differences and/or different growth metrics (e.g., linear extension and calcification). Linear extension is a plastic trait that can be influenced by factors like water flow and light while gross calcification rates remain the same (Jokiel 1978; Todd 2008; Kuffner et al. 2017). Moreover, linear extension rates may persist under shifts in carbonate chemistry even as calcification rates decline, reflecting a trade-off in which corals maintain extension at the expense of skeletal density (Fantazzini et al. 2015; Tambutté et al. 2015). This underscores the limitations of using linear extension alone to assess growth responses to eAE. In this light, our moderate growth enhancements offer a more comprehensive assessment of eAE's capacity to stimulate growth rates by integrating both calcification and linear extension metrics.

Further, eAE provides modest growth enhancements compared to other AE methods that have been tested in controlled laboratory settings. For instance, Langdon *et al.* (2000) observed threefold to twelvefold increases in coral calcification rates when Ω_{Ar} was enhanced with calcium or carbonate ion additions. Similarly, Herfort *et al.* (2008) reported four- to fivefold increases in calcification and photosynthesis rates by adding bicarbonate while maintaining pH at 8.2, and Marubini and Thake (1999) found roughly a doubling of coral growth under elevated DIC concentrations. These studies confirm corals' high capacity for accelerated calcification under favorable seawater carbonate chemistries. Our results did not achieve these high growth enhancements, likely because abiotic mineral precipitation at the cathodes competes for the electrochemically produced alkalinity, a symptom of runaway precipitation that ultimately results in less realized AE than is added to the system (*en sensu* Moras et al. 2022). Additionally, the lower growth enhancements observed with eAE may result from its selective enhancement of A_T without concurrent enhancements to DIC, whereas many mineral addition AE methods alter both A_T and DIC, e.g., CO_3^{2-} (Figure S7). Nevertheless, the observed 43% enhancement of calcification rates for short microfragments in our eAE system is consistent with a thermodynamic facilitation of calcification.

Chan and Connolly's (2013) meta-analysis of coral growth experiments with varying Ω_{Ar} predicted an approximate 15% change in calcification rates

per unit change of Ω_{Ar}. Accordingly, the modeled Ω_{Ar} within the pH boundary layer, assuming hydroxide ion production following the water reduction reaction, increased from 3.85 to 4.68 (Figure S7), yielding a predicted increase in calcification rates of 14%. Our observed enhancement (43%) exceeding this prediction is anticipated due to the nonlinear effect of Ω_{Ar} on calcification rates (Anthony et al. 2011). Moreover, Chan and Connolly's wide confidence interval (0-31% change in calcification rates per unit of Ω_{Ar}, most accurate between 2-4) suggests a possible maximum predicted growth increase of 37%, which more closely aligns with our observed enhancement. Additionally, using the equation fit by Langdon (2000) to a range of enhanced carbonate chemistries, our modeled Ω_{Ar} increase predicts an average calcification enhancement of 92%, ranging from 75-168%. Taken together, our calcification enhancements of small microfragments are in line with the enhanced Ω_{Ar} facilitation of calcification rates.

In contrast to the short microfragments, taller corals (≥ 15 mm) in our study showed no measurable growth benefit from eAE, an outcome that can be explained by the limited spatial extent of the pH boundary layer. Neither the tall *P. clivosa* fragments (15 mm) nor the branching *A. cervicornis* nubbins (50 mm) exhibited significant increases in calcification relative to their controls. In the *A. cervicornis* experiment, the increased mass gain on eAE substrates was entirely attributed to abiotic mineral precipitation on the cathode (Figure 3). Similarly, in the *P. clivosa* microfragment experiment, the tall fragments on eAE grew at the same rate as those on inert acrylic pucks (Figure 4).

Several lines of evidence support boundary-layer limitations as the explanation for why larger corals did not benefit from eAE. Our microelectrode measurements demonstrated that the eAE-induced pH elevation attenuated to bulk values within 15 mm of the cathode under flow speeds of 1 cm s^{-1} (Figure 2), and no changes in bulk carbonate chemistry were detected during either growth experiment (Table 1). The taller *P. clivosa* fragments and the actively calcifying tips of the *A. cervicornis* extended well beyond the enhanced microenvironment. Additionally, substantial cyanoacrylate glue was needed to affix the *A. cervicornis* branches to the cathodes, covering basal tissue and further limiting exposure to the elevated microenvironment. Thus, even the lowest portions of these corals remained outside of the alkalinity-enhanced layer and did not exhibit enhanced growth, unlike the basal regions observed in Sabater and Yap (2002), which were directly attached to the cathodes. Additionally, the limited spatial extent of eAE presents a temporal limitation, as corals can outgrow the enhanced microenvironment, explaining the transient benefits observed in the literature (Sabater and Yap 2004; Huang et al. 2020).

These results corroborate previous findings that enhanced growth rates are restricted to the basal portions of taller fragments or to fragments directly attached to cathodes without intervening epoxy layers, which both place the coral outside of the pH boundary layer (Sabater and Yap 2002; Samidon et al. 2022). Nevertheless, there are documented cases of larger

corals experiencing growth benefits from eAE (Damayanti et al. 2011; Natasasmita et al. 2016). Such discrepancies likely stem from differences in local environmental conditions, including flow speed, light availability, and cathode geometry. Our findings highlight water flow significantly governs eAE efficacy by modulating the thickness of the alkalinity-enhanced microenvironment. Under static conditions (0 cm s^{-1}), the elevated pH boundary layer reached approximately 20 mm in thickness but decreased to 15 mm at 1 cm s^{-1} and further to 5 mm at 3 cm s^{-1} (Figure 2). Enhanced mixing and advective transport from modest water flows rapidly diminish the microenvironment thickness, consistent with mass transfer theory and previous studies of benthic boundary layers (Jorgensen and Revsbech 1985; Shashar et al. 1996). Consequently, stronger flow speeds in field conditions are likely to decrease the boundary layer thickness, reducing eAE effectiveness. This aligns with observations by Natasasmita et al. (2016), who noted growth enhancements in larger fragments (3-5 cm) under relatively slow currents in their coral nursery.

Cathode geometry further influences boundary layer thickness. Many successful eAE field implementations use round, cage-like cathode structures that are likely to retain alkalinity more effectively than the flat-channel plates used in our experiments (e.g., Goreau et al. 2004; Damayanti et al. 2011). Our flow-mediated pH boundary layers above a flat plate are consistent with recent modeling by Lees *et al.* (2024), though our measured gradients were smaller, possibly due to unaccounted abiotic precipitation in their models. Ultimately, our results reinforce that eAE is spatially limited and most effective in low-flow environments suitable for smaller-sized corals or plating morphologies that can remain entirely within the elevated alkalinity boundary layer. This spatial limitation underscores the practical applicability of eAE primarily in sheltered, low-flow locations, such as land-based nurseries or back-reef zones with limited water exchange. Alternatively, selecting cathode geometries to reduce advective transport and retain alkalinity or tuning eAE to programmed or naturally occurring reduced water flow periods, e.g., tide cycles, could increase the feasibility of eAE in a wider range of environments.

Moreover, electrochemical system design plays a critical role in eAE performance and ecological stewardship. In addition to flow-mediated boundary layer thickness, the appropriate placement of the anode is essential to avoid introducing acidity and chlorine byproducts into the coral's environment. The anode produces acids and reactive chlorine species, which can be harmful to marine organisms (Eisaman et al. 2023). In our system, we housed the anode within a pump-driven siphon to evacuate acidity and chlorine gas. All corals survived the 60-day experiments and photochemical efficiency values were reflective of healthy corals, underscoring the negligible effects of eAE on coral health when oxidative reactions are isolated from the system. This is in contrast to some eAE deployments which observed declining survival rates on eAE structures (Romatzki 2014). Therefore, similar precautions would be necessary in both land and field applications,

for example positioning the anode downstream of prevailing currents. At larger operational scales required for effective coral restoration, containment, utilization, or treatment of electrochemical byproducts would be necessary to prevent environmental contamination. This challenge is already recognized in broader AE research for carbon dioxide removal, where integrated designs have been proposed to pair AE systems with industrial processes, capturing byproducts like chlorine and hydrogen gas for commercial use and energy generation (Eisaman et al. 2023; Taqieddin et al. 2024).

Further, the current density of the electrochemical system must be optimized. While higher current densities increase hydroxide ion production and enhance local alkalinity, they also accelerate abiotic precipitation of calcium carbonate, magnesium hydroxide (brucite), and anodic byproducts (Akamine and Kashiki 2002; Carré et al. 2020). The abiotic mineral precipitation can rapidly sequester the leached alkalinity, a process known as runaway precipitation whereby excessive alkalinity inputs trigger a disproportionate amount of mineral formation and lead to a net decrease in A_T (Moras et al. 2022). In our system, even at a moderate current density of 1 A m^{-2}, abiotic precipitation exceeded biological calcification rates by approximately 300% (Figure 4). Managing the trade-off between abiotic precipitation and biological calcification is critical, especially for small fragments that must remain in close contact with the cathode. While tipping points in current density that favor brucite over calcium carbonate precipitation have been documented (Akamine and Kashiki 2002; Devi et al. 2025), similar investigations are needed to determine optimal current densities for effective eAE applications. The electrical current densities investigated in this study fell in line with those reported by other studies (e.g., Borell et al. 2010), though some studies employed current densities orders of magnitude less (e.g., Kihara et al. 2013; Huang et al. 2020). However, many published studies on eAE do not report the electrical current density used in their systems, limiting comparability and reproducibility.

Despite its constraints, eAE shows promise as a complementary technology to existing restoration methods and can enhance coral growth rates in field and land-based nurseries. Microfragmentation—a technique in which corals are cut into small fragments to maximize growth efficiency—has been widely adopted in restoration nurseries due to its ability to accelerate lateral tissue growth and generate a high number of outplantable units (Forsman et al. 2015; Page et al. 2018). In our study, microfragments exposed to eAE exhibited up to 50% greater planar tissue growth than controls, suggesting that combining eAE with microfragmentation could further enhance growth rates and skirting morphology, reducing grow-out time in nurseries and increasing biomass production. Further, microfragments remain highly susceptible to post-outplant mortality, primarily due to predation by fish and other grazers (Page et al. 2018; Koval et al. 2020; Rivas et al. 2021). Their small size disproportionately amplifies the effects of partial mortality and tissue loss shortly after deployment. By accelerating

microfragment growth in nurseries, eAE may help microfragments reach larger, less vulnerable size classes more quickly, potentially improving their survivorship post-outplant. Additional studies are needed to evaluate whether growth enhancements observed in controlled settings translate to improved outcomes in the field.

Moreover, eAE may enhance coral breeding efforts, a multifaceted endeavor that involves crossing gametes, culturing larvae, and propagating lab-reared offspring, which themselves can be introduced back into a selective breeding pipeline (Banaszak et al. 2023). While these efforts yield thousands of genetically diverse individuals, survivorship remains a major bottleneck, with fewer than 3% of settled spat typically surviving their first year (Wilson and Harrison 2005; Vermeij and Sandin 2008). Additionally, even fast-growing species such as Acropora require at least four years to reach reproductive maturity (Chamberland et al. 2016), limiting the scalability of assisted evolution strategies that rely on multi-generational selection (Van Oppen et al. 2015). By enhancing growth rates during early life stages, eAE may accelerate the sexual maturation of propagated corals, enabling shorter breeding cycles and improving throughput in selective propagation efforts.

In addition to enhancing coral growth, the abiotic precipitation generated by eAE may serve a structural function by contributing calcium carbonate material that can stabilize loose reef rubble. The abiotically formed aragonite produces a carbonate substrate with physical and chemical properties comparable to natural coral skeletons (Margheritini et al. 2021). This mineral accretion can act as a binding agent, cementing unconsolidated substrates into more stable frameworks (Landivar Macias et al. 2024). Such stabilization is particularly valuable in degraded reef environments where rubble movement inhibits coral recruitment and survivorship (Ceccarelli et al. 2020). However, systems intended for rubble stabilization need to be designed distinctly from those optimized for coral growth, as the target product shifts from soluble alkalinity delivery to sustained mineral accretion and substrate binding.

In conclusion, eAE shows clear potential to accelerate the growth of small corals, particularly microfragments and juvenile corals, making it a valuable tool for restoration nurseries. Realizing its full potential will require further research into long-term efficacy, species-specific responses, system design, practical deployment, and integration with existing technologies. Addressing these knowledge gaps and engineering hurdles will help refine eAE implementation within coral propagation pipelines. With continued development, eAE is poised to become a complementary technique to enhance coral growth rates and ultimately increase the scale of restoration.

Data Availability

All data and scripts are publicly available on Github (Kiel 2025).

Contributions

P.M.K. contributed to conceptualization, funding acquisition, methodology, investigation, data analysis, writing—original draft, and visualization. M.M. contributed to methodology, investigation, and data analysis. A.B., N.S. contributed to methodology and investigation. V.N.P., I.C.E., and P.S. contributed to conceptualization, supervision, and funding acquisition. All authors reviewed and edited the manuscript.

Figures

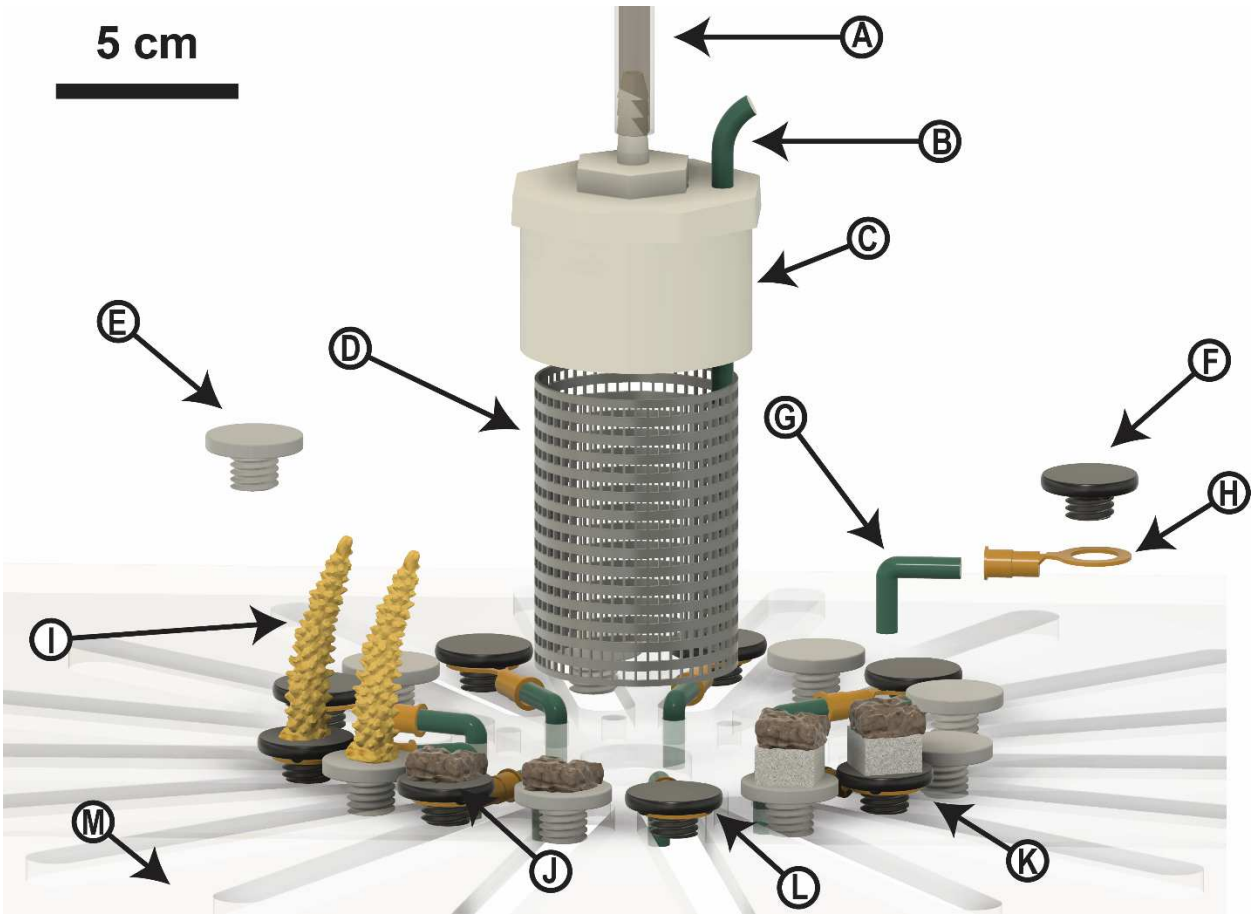

Figure 1. Diagram of the electrochemically induced alkalinity enhancement (eAE) system. The system includes an **(A)** evacuation hose and **(B)** anode wire integrated into a **(C)** PVC anode pump, which surrounds a **(D)** mesh anode to evacuate oxidizing products. **(E)** Inert acrylic pucks and **(F)** steel cathodes are arranged around the anode and are connected to the electrochemical system via **(G)** cathode wires and **(H)** ring terminals. The system was tested with **(I)** five-centimeter *Acropora cervicornis* fragments, **(J)** short, five-millimeter and **(K)** tall, fifteen-millimeter *Pseudodiploria clivosa* microfragments grown on E and F and **(L)** bare eAE cathodes. The system was mounted to **(M)** an acrylic stage to keep cathodes equidistantly spaced from the anode in a circular pattern. The PVC anode pump and evacuation hose are shortened for illustrative purposes only (Figure S1).

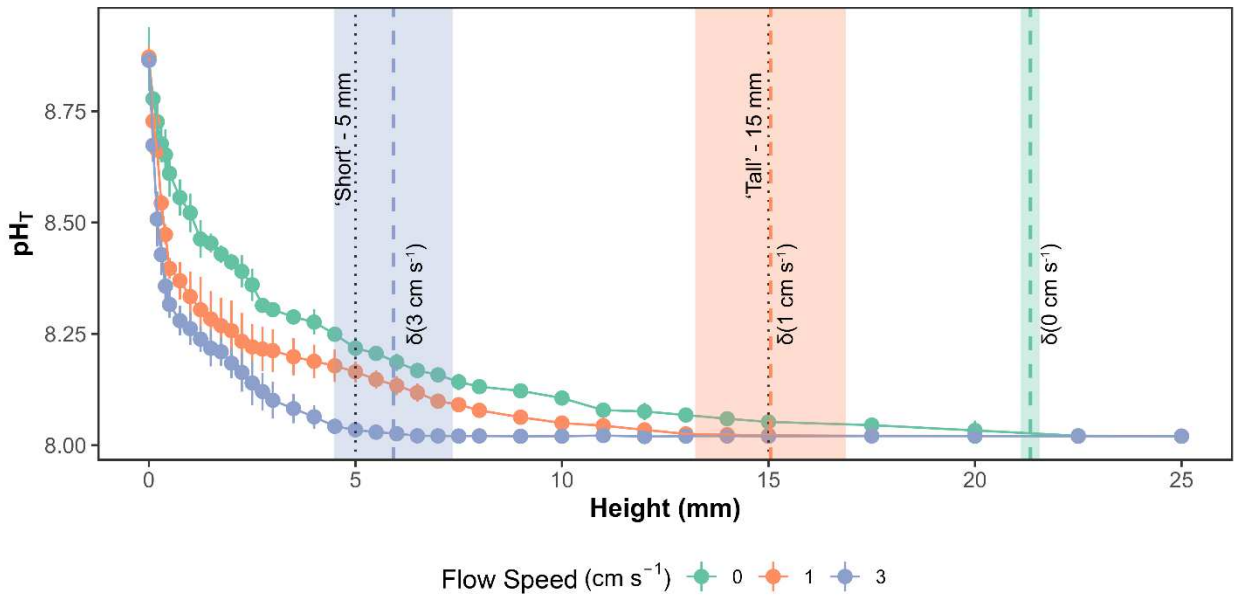

Figure 2. pH microsensor profiles above eAE substrates at three distinct flow speeds (cm s^{-1}), each operated at 1 A m^{-2}. Vertical line segments centered on each point indicate ± 1 standard deviation (SD) about the mean. Vertical dashed lines with surrounding ribbons represent the mean ± 1 SD of the pH boundary layer heights (δ) derived from the hyperbolic tangent model for each flow speed. Vertical dotted lines at 5 mm (short) and 15 mm (tall) mark the fragment heights of the *P. clivosa* corals used in the microfragment experiment.

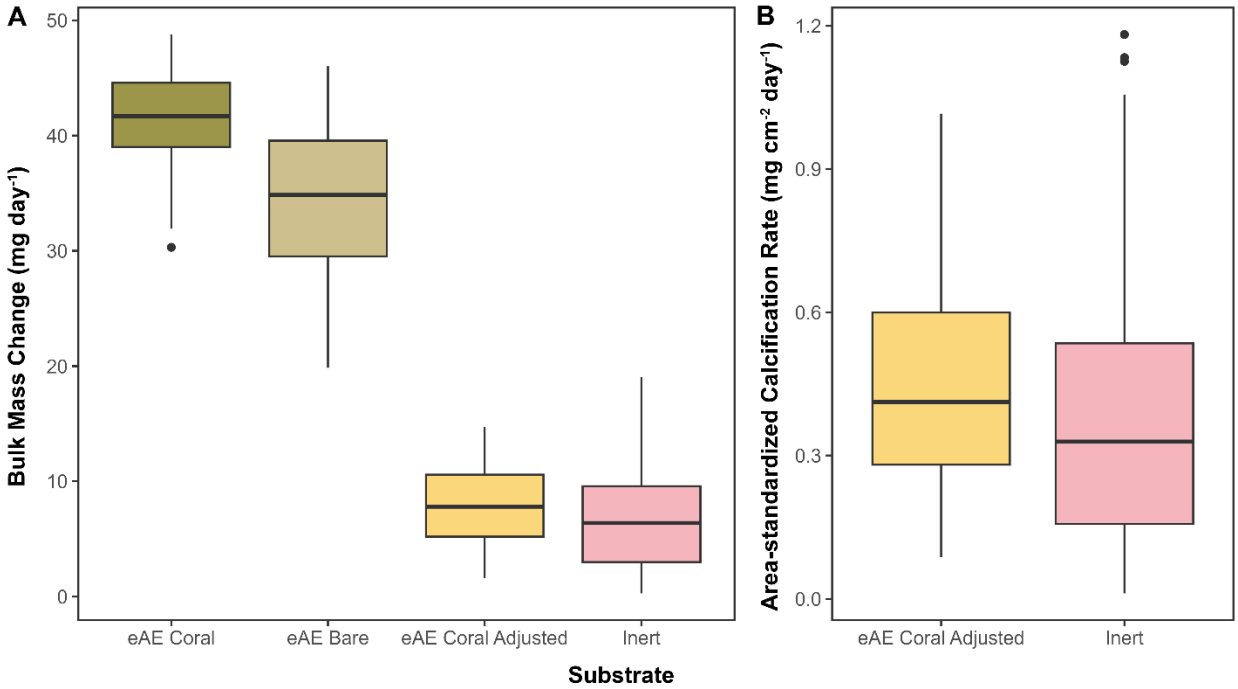

Figure 3. *A. cervicornis* **(A)** bulk mass change rates (mg day^{-1}) and **(B)** area-standardized daily calcification rates (mg cm^{-2} day^{-1}), including corals grown

on eAE substrates (eAE Coral), abiotic precipitation from bare eAE substrates (eAE Bare), eAE Corals adjusted for abiotic precipitation by subtracting the average eAE Bare value from the eAE Coral value (eAE Coral Adjusted), and corals grown on inert acrylic pucks (Inert).

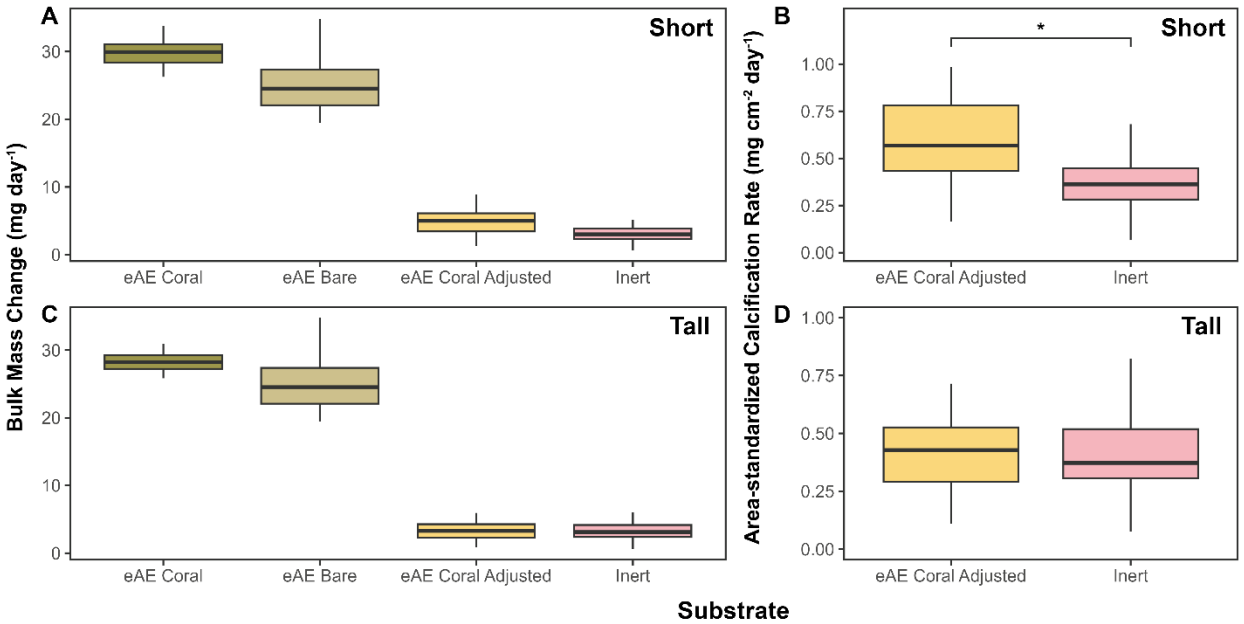

Figure 4. *P. clivosa* **(A, C)** bulk mass change rates (mg day^{-1}) and **(B, D)** area-standardized daily calcification rates (mg cm^{-2} day^{-1}) for short and tall microfragments, including corals grown on eAE substrates (eAE Coral), abiotic precipitation from bare eAE substrates (eAE Bare), eAE Corals adjusted for abiotic precipitation by subtracting the average eAE Bare value from the eAE Coral value (eAE Coral Adjusted), and corals grown on inert acrylic pucks (Inert); * denotes significant differences at $p < 0.05$.

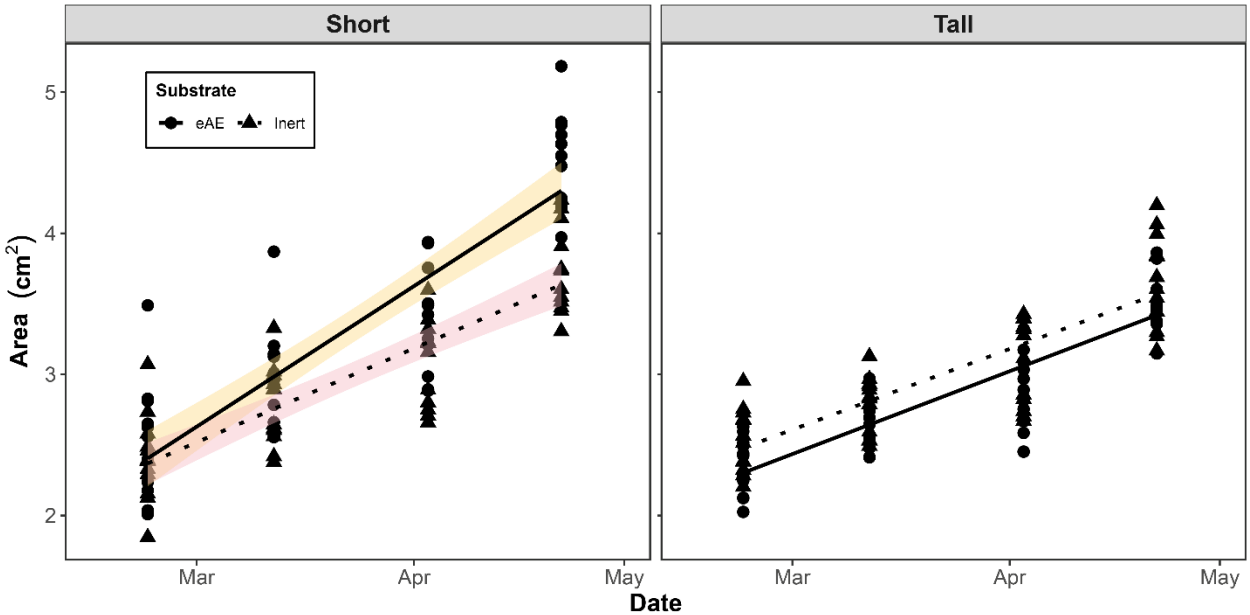

Figure 5. *P. clivosa* planar area growth rates for microfragments on eAE substrates (circles) and inert acrylic pucks (triangles). The slopes of the lines indicate the average planar tissue growth rates for the eAE corals (solid) and for the corals grown on inert acrylic pucks (dotted). Standard errors are only displayed for lines that have significantly different slopes ($p < 0.0001$) within a fragment height class.

Tables

Table 1. Carbonate chemistry data measured from the two coral growth experiments, represented as mean ± 1SD. pH_T refers to the spectrophotometrically measured pH. † denotes significant differences between experiments at $p < 1e-7$.

Species	***Aquarium***	***Treat***	***Temp (°C)***	***Sal (psu)***	***DIC (µmol kg^{-1})***	***TA (µmol kg^{-1})***	***pH_T***	***CO_2† (µmol kg^{-1})***	***pCO_2† (ppm)***	***HCO_3^- (µmol kg^{-1})***	***CO_3^{2-}† (µmol kg^{-1})***	***Ω_{Ar}†***
A. cervicornis	**Total**		27.97 ± 0.05	34.38 ± 0.79	2113 ± 33	2420 ± 24	8.00 ± 0.04	13 ± 2	476 ± 58	1877 ± 44	225 ± 16	3.63 ± 0.27
	T5	**eAE**	27.96 ± 0.06	34.32 ± 0.82	2119 ± 34	2424 ± 23	8.00 ± 0.03	13 ± 2	482 ± 60	1883 ± 46	223 ± 16	3.61 ± 0.27
	T6	**eAE**	27.97 ± 0.04	34.50 ± 0.87	2105 ± 32	2418 ± 27	8.02 ± 0.04	12 ± 2	465 ± 59	1865 ± 42	228 ± 17	3.70 ± 0.29
	T7	**eAE**	27.96 ± 0.05	34.34 ± 0.77	2117 ± 35	2421 ± 24	8.00 ± 0.05	13 ± 2	483 ± 63	1882 ± 47	222 ± 17	3.60 ± 0.29
	T8	**eAE**	27.98 ± 0.06	34.35 ± 0.82	2114 ± 34	2422 ± 25	8.01 ± 0.04	13 ± 2	475 ± 58	1877 ± 45	224 ± 17	3.64 ± 0.26

P. clivosa	**Total**		27.85 ± 0.39	33.48 ± 1.12	2099 ± 53	2457 ± 37	8.10 ± 0.07	10 ± 2	382 ± 63	1828 ± 69	261 ± 24	4.24 ± 0.41
	TTB1	**eAE**	27.83 ± 0.41	33.50 ± 1.20	2107 ± 68	2461 ± 36	8.08 ± 0.09	11 ± 2	394 ± 83	1839 ± 92	258 ± 30	4.20 ± 0.52
	TTB2	**control**	27.78 ± 0.38	33.48 ± 1.18	2113 ± 56	2451 ± 40	8.07 ± 0.07	11 ± 2	413 ± 59	1855 ± 68	247 ± 18	4.01 ± 0.33
	TTD1	**control**	27.93 ± 0.41	33.48 ± 1.16	2093 ± 46	2455 ± 43	8.11 ± 0.08	10 ± 1	374 ± 48	1820 ± 54	263 ± 19	4.28 ± 0.34
	TTD2	**eAE**	27.75 ± 0.52	33.47 ± 1.21	2083 ± 47	2463 ± 38	8.13 ± 0.05	9 ± 1	347 ± 50	1799 ± 59	275 ± 20	4.47 ± 0.35

References

Akamine K, Kashiki I (2002) Corrosion Protection of Steel by Calcareous Electrodeposition in Seawater (Part 1). Corrosion Engineering 51:496–501. https://doi.org/10.3323/jcorr1991.51.496

Albright R, Caldeira L, Hosfelt J, Kwiatkowski L, Maclaren JK, Mason BM, Nebuchina Y, Ninokawa A, Pongratz J, Ricke KL, Rivlin T, Schneider K, Sesboüé M, Shamberger K, Silverman J, Wolfe K, Zhu K, Caldeira K (2016) Reversal of ocean acidification enhances net coral reef calcification. Nature 531:362–365. https://doi.org/10.1038/nature17155

Alvarez-Filip L, Dulvy NK, Gill JA, Côté IM, Watkinson AR (2009) Flattening of Caribbean coral reefs: Region-wide declines in architectural complexity. Proceedings of the Royal Society B: Biological Sciences 276:3019–3025. https://doi.org/10.1098/rspb.2009.0339

Anthony KRN, A. Kleypas J, Gattuso JP (2011) Coral reefs modify their seawater carbon chemistry - implications for impacts of ocean acidification. Global Change Biology 17:3655–3666. https://doi.org/10.1111/j.1365-2486.2011.02510.x

Banaszak AT, Marhaver KL, Miller MW, Hartmann AC, Albright R, Hagedorn M, Harrison PL, Latijnhouwers KRW, Mendoza Quiroz S, Pizarro V, Chamberland VF (2023) Applying coral breeding to reef restoration: best practices, knowledge gaps, and priority actions in a rapidly-evolving field. Restoration Ecology 31:e13913. https://doi.org/10.1111/rec.13913

Bard AJ, Faulkner LR (2001) Electrochemical Methods: Fundamentals and Applications. John Wiley & Sons, Inc.,

Borell EM, Romatzki SBC, Ferse SCA (2010) Differential physiological responses of two congeneric scleractinian corals to mineral accretion and an electric field. Coral Reefs 29:191–200. https://doi.org/10.1007/s00338-009-0564-y

Boström-Einarsson L, Babcock RC, Bayraktarov E, Ceccarelli D, Cook N, Ferse SCA, Hancock B, Harrison P, Hein M, Shaver E, Smith A, Suggett D, Stewart-Sinclair PJ, Vardi T, McLeod IM (2020) Coral restoration – A systematic review of current methods, successes, failures and future directions. PLoS ONE 15:e0226631. https://doi.org/10.1371/journal.pone.0226631

Carré C, Zanibellato A, Jeannin M, Sabot R, Gunkel-Grillon P, Serres A (2020) Electrochemical calcareous deposition in seawater. A review.

Environ Chem Lett 18:1193–1208. https://doi.org/10.1007/s10311-020-01002-z

Ceccarelli DM, McLeod IM, Boström-Einarsson L, Bryan SE, Chartrand KM, Emslie MJ, Gibbs MT, Rivero MG, Hein MY, Heyward A, Kenyon TM, Lewis BM, Mattocks N, Newlands M, Schläppy M-L, Suggett DJ, Bay LK (2020) Substrate stabilisation and small structures in coral restoration: State of knowledge, and considerations for management and implementation. PLOS ONE 15:e0240846. https://doi.org/10.1371/journal.pone.0240846

Chamberland V, Petersen D, Latijnhouwers K, Snowden S, Mueller B, Vermeij MJA (2016) Four-year-old Caribbean Acropora colonies reared from field-collected gametes are sexually mature. Bulletin of Marine Science 92:e1074. https://doi.org/10.5343/bms.2015.1074

Chan NCS, Connolly SR (2013) Sensitivity of coral calcification to ocean acidification: a meta-analysis. Global Change Biology 19:282–290. https://doi.org/10.1111/gcb.12011

Chavanich S, Ussavauschariyakul S, Viyakarn V, Fujita T (2015) Influence of mineral accretion induced by electric current on the settlement and growth of the scleractinian coral Pocillopora damicornis. Mar Res Indonesia 38:89–94. https://doi.org/10.14203/mri.v38i2.60

Damayanti LPA, Ahyadi H, Candri DA, Sabil A (2011) Growth Rate of Acropora formosa and Montipora digitata transplanted on biorock in Gili Trawangan. Journal of Indonesia Coral Reefs 1:114–119.

DeMerlis A, Kirkland A, Kaufman ML, Mayfield AB, Formel N, Kolodzeij G, Manzello DP, Lirman D, Traylor-Knowles N, Enochs IC (2022) Pre-exposure to a variable temperature treatment improves the response of Acropora cervicornis to acute thermal stress. Coral Reefs 41:435–445. https://doi.org/10.1007/s00338-022-02232-z

Devi N, Gong X, Shoji D, Wagner A, Guerini A, Zampini D, Lopez J, Rotta Loria AF (2025) Electrodeposition of carbon-trapping minerals in seawater for variable electrochemical potentials and carbon dioxide injections. Advanced Sustainable Systems 9:2400943. https://doi.org/10.1002/adsu.202400943

Eisaman MD, Geilert S, Renforth P, Bastianini L, Campbell J, Dale AW, Foteinis S, Grasse P, Hawrot O, Löscher CR, Rau GH, Rønning J (2023) Assessing the technical aspects of ocean-alkalinity-enhancement approaches. State of the Planet 2-oae2023:1–29. https://doi.org/10.5194/sp-2-oae2023-3-2023

Enochs IC, Manzello DP, Carlton RD, Schopmeyer S, van Hooidonk R, Lirman D (2014) Effects of light and elevated pCO2 on the growth and photochemical efficiency of Acropora cervicornis. Coral Reefs 33:477–485. https://doi.org/10.1007/s00338-014-1132-7

Enochs IC, Manzello DP, Jones P, Aguilar C, Cohen K, Valentino L, Schopmeyer S, Kolodzeij G, Jankulak M, Lirman D (2018) The influence of diel carbonate chemistry fluctuations on the calcification rate of Acropora cervicornis under present day and future acidification conditions. Journal of Experimental Marine Biology and Ecology 506:135–143. https://doi.org/10.1016/j.jembe.2018.06.007

Enochs IC, Manzello DP, Jones PR, Stamates SJ, Carsey TP (2019) Seasonal carbonate chemistry dynamics on southeast Florida coral reefs: localized acidification hotspots from navigational inlets. Frontiers in Marine Science 6:160. https://doi.org/10.3389/fmars.2019.00160

Enochs IC, Studivan MS, Kolodziej G, Foord C, Basden I, Boyd A, Formel N, Kirkland A, Rubin E, Jankulak M, Smith I, Kelble CR, Manzello DP (2023) Coral persistence despite marginal conditions in the Port of Miami. Sci Rep 13:6759. https://doi.org/10.1038/s41598-023-33467-7

Fantazzini P, Mengoli S, Pasquini L, Bortolotti V, Brizi L, Mariani M, Di Giosia M, Fermani S, Capaccioni B, Caroselli E, Prada F, Zaccanti F, Levy O, Dubinsky Z, Kaandorp JA, Konglerd P, Hammel JU, Dauphin Y, Cuif JP, Weaver JC, Fabricius KE, Wagermaier W, Fratzl P, Falini G, Goffredo S (2015) Gains and losses of coral skeletal porosity changes with ocean acidification acclimation. Nature Communications 6:7785. https://doi.org/10.1038/ncomms8785

Forsman ZH, Page CA, Toonen RJ, Vaughan D (2015) Growing coral larger and faster: micro-colony-fusion as a strategy for accelerating coral cover. PeerJ 3:e1313. https://doi.org/10.7717/peerj.1313

Gattuso JP, Epitalon J-M, Lavigne H, Orr J (2024) seacarb. https://CRAN.R-project.org/package=seacarb

Goreau TJ (2013) Innovative methods of marine ecosystem restoration. CRC Press, Boca Raton, Florida

Goreau TJ, Cervin JM, Pollina R (2004) Increased zooxanthellae numbers and mitotic index in electrically stimulated corals. Symbiosis 37:107–120.

Goreau TJF (2022) Coral reef electrotherapy: field observations. Frontiers in Marine Science 9:https://doi.org/10.3389/fmars.2022.805113

Graham NAJ, Nash KL (2013) The importance of structural complexity in coral reef ecosystems. Coral Reefs 32:315–326. https://doi.org/10.1007/s00338-012-0984-y

Herfort L, Thake B, Taubner I (2008) Bicarbonate stimulation of calcification and photosynthesis in two hermatypic corals. Journal of Phycology 44:91–98. https://doi.org/10.1111/j.1529-8817.2007.00445.x

Hilbertz WH, Goreau TJ (1996) Method of enhancing the growth of aquatic organisms, and structures created thereby. https://patents.google.com/patent/US5543034A/en

Huang B, Yuan T, Liang Y, Guo Y, Yuan X, Zhou W, Huang H, Liu S (2020) Low electric current density enhances the calcification rate of the colonial stony coral Galaxea fascicularis. Aquatic Ecosystem Health & Management 23:332–340. https://doi.org/10.1080/14634988.2020.1768766

Hurd CL, Cornwall CE, Currie K, Hepburn CD, McGraw CM, Hunter KA, Boyd PW (2011) Metabolically induced pH fluctuations by some coastal calcifiers exceed projected 22nd century ocean acidification: a mechanism for differential susceptibility? Global Change Biology 17:3254–3262. https://doi.org/10.1111/j.1365-2486.2011.02473.x

Jokiel PL (1978) Effects of water motion on reef corals. Journal of Experimental Marine Biology and Ecology 35:87–97. https://doi.org/10.1016/0022-0981(78)90092-8

Jokiel PL, Maragos JE, Franzisket L (1978) Coral growth: buoyant weight technique. In: Stoddart D.R., Johannes R.E. (eds) Coral reefs: research methods. UNESCO, Paris, France, pp 529–541.

Jorgensen BB, Revsbech NP (1985) Diffusive boundary layers and the oxygen uptake of sediments and detritus. Limnology and Oceanography 30:111–122. https://doi.org/10.4319/lo.1985.30.1.0111

Kiel PM (2025) pkiel/eAE. https://github.com/pkiel/eAE

Kihara K, Taniguchi H, Koibuchi Y, Yamamoto S, Kondo Y, Hosokawa Y (2013) Enhancing settlement and growth of corals using feeble electrochemical method. Galaxea, Journal of Coral Reef Studies 15:323–329. https://doi.org/10.3755/galaxea.15.323

Kleypas JA, Allemand D, Anthony KRN, Baker AC, Beck MW, Hale LZ, Hilmi N, Hoegh-Guldberg O, Hughes T, Kaufman L, Kayanne H, Magnan AK, Mcleod E, Mumby P, Palumbi SR, Richmond RH, Rinkevich B, Steneck

RS, Voolstra CR, Wachenfeld D, Gattuso JP (2021) Designing a blueprint for coral reef survival. Biological Conservation 257:109107. https://doi.org/10.1016/j.biocon.2021.109107

Koval G, Rivas N, D'Alessandro M, Hesley D, Santos R, Lirman D (2020) Fish predation hinders the success of coral restoration efforts using fragmented massive corals. PeerJ 8:e9978. https://doi.org/10.7717/peerj.9978

Kuffner IB, Bartels E, Stathakopoulos A, Enochs IC, Kolodzeij G, Toth LT, Manzello DP (2017) Plasticity in skeletal characteristics of nursery-raised staghorn coral, Acropora cervicornis. Coral Reefs 36:679–684. https://doi.org/10.1007/s00338-017-1560-2

Landivar Macias A, Jacobsen SD, Rotta Loria AF (2024) Electrodeposition of calcareous cement from seawater in marine silica sands. Commun Earth Environ 5:442. https://doi.org/10.1038/s43247-024-01604-3

Langdon C, Takahashi T, Sweeney C, Chipman D, Goddard J, Marubini F, Aceves H, Barnett H, Atkinson MJ (2000) Effect of calcium carbonate saturation state on the calcification rate of an experimental coral reef. Global Biogeochemical Cycles 14:639–654. https://doi.org/10.1029/1999GB001195

Lees EW, Tournassat C, Weber AZ, Gilbert PUPA (2024) eCoral: how electrolysis could restore seawater conditions ideal for coral reefs. J Phys Chem Lett 15:12206–12211. https://doi.org/10.1021/acs.jpclett.4c02715

Margheritini L, Møldrup P, Jensen RL, Frandsen KM, Antonov YI, Kawamoto K, de Jonge LW, Vaccarella R, Bjørgård TL, Simonsen ME (2021) Innovative material can mimic coral and boulder reefs properties. Frontiers in Marine Science 8:652986. https://doi.org/10.3389/fmars.2021.652986

Marubini F, Thake B (1999) Bicarbonate addition promotes coral growth. Limnology and Oceanography 44:716–720. https://onlinelibrary.wiley.com/doi/abs/10.4319/lo.1999.44.3.0716

Moras CA, Bach LT, Cyronak T, Joannes-Boyau R, Schulz KG (2022) Ocean alkalinity enhancement – avoiding runaway CaCO3 precipitation during quick and hydrated lime dissolution. Biogeosciences 19:3537–3557. https://doi.org/10.5194/bg-19-3537-2022

Natasasmita D, Wijayanti DP, Suryono CA (2016) The effects of electrical voltage differences and initial fragment size on growth performance and survival rate of coral Acropora cerealis in biorock method. Journal

of Aquaculture & Marine Biology 4:e11-12. https://doi.org/10.15406/jamb.2016.04.00086

Nishihara GN, Ackerman JD (2007) On the determination of mass transfer in a concentration boundary layer. Limnology and Oceanography: Methods 5:88–96. https://doi.org/10.4319/lom.2007.5.88

NOAA (2024) Precipitation Data at Miami International Airport. https://www.ncdc.noaa.gov/cdo-web/datasets/GHCND/stations/GHCND:USW00012839/detail

Page CA, Muller EM, Vaughan DE (2018) Microfragmenting for the successful restoration of slow growing massive corals. Ecological Engineering 123:86–94. https://doi.org/10.1016/j.ecoleng.2018.08.017

Palacio-Castro AM, Rosales SM, Dennison CE, Baker AC (2022) Microbiome signatures in Acropora cervicornis are associated with genotypic resistance to elevated nutrients and heat stress. Coral Reefs 41:1389–1403. https://doi.org/10.1007/s00338-022-02289-w

Perry CT, Murphy GN, Kench PS, Smithers SG, Edinger EN, Steneck RS, Mumby PJ (2013) Caribbean-wide decline in carbonate production threatens coral reef growth. Nature Communications 4:1402. https://doi.org/10.1038/ncomms2409

R Core Team (2024) R: A language and environment for statistical computing. R Foundation for Statistical Computing https://www.r-project.org/

Rivas N, Hesley D, Kaufman M, Unsworth J, D'Alessandro M, Lirman D (2021) Developing best practices for the restoration of massive corals and the mitigation of predation impacts: influences of physical protection, colony size, and genotype on outplant mortality. Coral Reefs 40:1227–1241. https://doi.org/10.1007/s00338-021-02127-5

Romatzki SBC (2014) Influence of electrical fields on the performance of Acropora coral transplants on two different designs of structures. Marine Biology Research 10:449–459. https://doi.org/10.1080/17451000.2013.814794

Ruszczyk M, Kiel PM, Chandragiri S, Guigand CM, Xia J, Brown O, Haus BK, Baker AC, Miller MW, Suraneni P, Langdon C, Prakash VN (2024) Flumex: A Modular Flume Design for Laboratory-Based Marine Fluid-Substrate Studies. https://papers.ssrn.com/abstract=5050355

Ruszczyk M, Rodriguez S, Tuen M, Rux K, Chandragiri S, Stickley M, Haus BK, Baker AC, Miller MW, Suraneni P, Langdon C, Prakash VN (2025)

Local alkalinity enhancement using artificial substrates increases survivorship of early-stage coral recruits. https://www.biorxiv.org/content/10.1101/2025.01.07.631763v1

Sabater MG, Yap HT (2002) Growth and survival of coral transplants with and without electrochemical deposition of CaCO3. Journal of Experimental Marine Biology and Ecology 272:131–146. https://doi.org/10.1016/S0022-0981(02)00051-5

Sabater MG, Yap HT (2004) Long-term effects of induced mineral accretion on growth, survival and corallite properties of Porites cylindrica Dana. Journal of Experimental Marine Biology and Ecology 311:355–374. https://doi.org/10.1016/j.jembe.2004.05.013

Samidon M, Razi NM, Agustiar M, Harahap PB, Najmi N, Bahri S, Liu SYV (2022) In-situ electro-stimulation enhanced branching but not massive scleractinian coral growth. Frontiers in Marine Science 9:https://doi.org/10.3389/fmars.2022.917360

Schindelin J, Arganda-Carreras I, Frise E, Kaynig V, Longair M, Pietzsch T, Preibisch S, Rueden C, Saalfeld S, Schmid B, Tinevez J-Y, White DJ, Hartenstein V, Eliceiri K, Tomancak P, Cardona A (2012) Fiji: an open-source platform for biological-image analysis. Nat Methods 9:676–682. https://doi.org/10.1038/nmeth.2019

Schoepf V, Cornwall CE, Pfeifer SM, Carrion SA, Alessi C, Comeau S, McCulloch MT (2018) Impacts of coral bleaching on pH and oxygen gradients across the coral concentration boundary layer: a microsensor study. Coral Reefs 37:1169–1180. https://doi.org/10.1007/s00338-018-1726-6

Schoepf V, Hu X, Holcomb M, Cai WJ, Li Q, Wang Y, Xu H, Warner ME, Melman TF, Hoadley KD, Pettay DT, Matsui Y, Baumann JH, Grottoli AG (2017) Coral calcification under environmental change: a direct comparison of the alkalinity anomaly and buoyant weight techniques. Coral Reefs 36:13–25. https://doi.org/10.1007/s00338-016-1507-z

Shashar N, Kinane S, Jokiel PL, Patterson MR (1996) Hydromechanical boundary layers over a coral reef. Journal of Experimental Marine Biology and Ecology 199:17–28. https://doi.org/10.1016/0022-0981(95)00156-5

Smith SV, Kinsey DW (1978) Calcification and organic carbon metabolism as indicated by carbon dioxide. In: Stoddart D.R., Johannes R.E. (eds) Coral reefs: research methods. UNESCO, Paris, France, pp 469–484.

Strömberg SM, Lundälv T, Goreau TJ (2010) Suitability of mineral accretion as a rehabilitation method for cold-water coral reefs. Journal of Experimental Marine Biology and Ecology 395:153–161. https://doi.org/10.1016/j.jembe.2010.08.028

Tambutté E, Venn AA, Holcomb M, Segonds N, Techer N, Zoccola D, Allemand D, Tambutté S (2015) Morphological plasticity of the coral skeleton under CO2-driven seawater acidification. Nature Communications 6:7368. http://doi.org/10.1038/ncomms8368

Taqieddin A, Sarrouf S, Ehsan MF, Buesseler K, Alshawabkeh AN (2024) Electrochemical ocean iron fertilization and alkalinity enhancement approach toward CO2 sequestration. npj Ocean Sustain 3:28. https://doi.org/10.1038/s44183-024-00064-8

Todd PA (2008) Morphological plasticity in scleractinian corals. Biological Reviews 83:315–337. https://doi.org/10.1111/j.1469-185X.2008.00045.x

Torres-Pulliza D, Dornelas MA, Pizarro O, Bewley M, Blowes SA, Boutros N, Brambilla V, Chase TJ, Frank G, Friedman A, Hoogenboom MO, Williams S, Zawada KJA, Madin JS (2020) A geometric basis for surface habitat complexity and biodiversity. Nature Ecology & Evolution 4:1495–1501. https://doi.org/10.1038/s41559-020-1281-8

Van Oppen MJH, Oliver JK, Putnam HM, Gates RD (2015) Building coral reef resilience through assisted evolution. Proceedings of the National Academy of Sciences 112:2307–2313. https://doi.org/10.1073/pnas.1422301112

Vermeij MJA, Sandin SA (2008) Density-dependent settlement and mortality structure the earliest life phases of a coral population. Ecology 89:1994–2004. https://doi.org/10.1890/07-1296.1

Webb AE, Enochs IC, Hooidonk RV, Westen RMV, Besemer N, Kolodziej G, Viehman TS, Manzello DP (2023) Restoration and coral adaptation delay, but do not prevent, climate-driven reef framework erosion of an inshore site in the Florida Keys. Scientific Reports 13:258. https://doi.org/10.1038/s41598-022-26930-4

Willauer HD, DiMascio F, Hardy DR, Williams FW (2014) Feasibility of CO2 extraction from seawater and simultaneous hydrogen gas generation using a novel and robust electrolytic cation exchange module based on continuous electrodeionization technology. Ind Eng Chem Res 53:12192–12200. https://doi.org/10.1021/ie502128x

Wilson J, Harrison P (2005) Post-settlement mortality and growth of newly settled reef corals in a subtropical environment. Coral Reefs 24:418–421. https://doi.org/10.1007/s00338-005-0033-1

Young CN, Schopmeyer SA, Lirman D (2012) A review of reef restoration and coral propagation using the threatened genus Acropora in the Caribbean and western Atlantic. Bulletin of Marine Science 88:1075–1098. https://doi.org/10.5343/bms.2011.1143

Supplementary Materials

Supplementary Methods

pH microprofiling

pH profiles were measured with a microprofiling system equipped with a pH microelectrode (pH-50, tip diameter 40-60 µm, spatial resolution 75-150 µm, response time <10 s; Unisense) and an external reference electrode (Radiometer analytical), calibrated daily with NBS buffers. The reference electrode was positioned orthogonally to a reference line connecting the cathode and anode to minimize interference from the electrolysis system. Values of pH_{NBS} were converted to pH_T using seacarb by first converting to the seawater-scale (pHnbs2sws) and subsequently to the total scale (pHconv) using the default arguments. Microelectrodes were connected to a multimeter (fx-6 UniAmp, Unisense) and continuously recorded at 0.33 Hz with the Unisense SensorTrace software. The microelectrode tip was initially positioned in the center of the cathode at the electrode surface with the aid of a camera connected to a macroscopic lens and moved vertically upward into the water column with a micromanipulator (MM33-2, Unisense). Based on the analysis of preliminary profiles, a protocol was defined with 100 µm steps between 0-500 µm, 250 µm steps between 500-3,000 µm, 500 µm steps between 3,000-8,000 µm, 1,000 µm steps between 8,000-15,000 µm, and 2,500 µm steps between 15,000-25,000 µm for a total of 37 steps spanning 2.5 cm for each profile. Each step took a total of 45 seconds, with 5 s to move between steps, 10 s for the sensor measurement to stabilize, and 30 s of measuring at 0.33 Hz, granting a total profiling time of approximately 30 minutes. Due to the lack of measured pH changes above the inert substrates during preliminary analysis, a simplified protocol was defined with 250 µm steps between 0-500 µm, 500 µm steps between 500-5,000 µm, 1,000 µm steps between 5,000-10,000 µm and 5,000 µm steps between 10,000-25,000 µm. Treatment of the inert and eAE profiles were otherwise identical. The 10 measurements at each step were averaged and taken as the individual step pH. Profiles were recentered to account for the small variation among replicate profiles by first converting to H^+ concentration, using the conversion $[H^+] = 10^{-pH}$, then dividing the concentration at any given step by the mean of the profile's bulk seawater $[H^+]$, defined by the average of the final three steps. This non-dimensional $[H^+]$ was then multiplied by the mean of all the profile's bulk $[H^+]$ to convert back to a standardized $[H^+]$ and back to pH units prior to further analysis (Hurd et al. 2011; Schoepf et al. 2018).

Alternative boundary layer height derivations

We analyzed four methods commonly used to determine the boundary layer height from the pH microprofiles including the intersection of the profile with 99% of the bulk concentration, intersection of the profile to its

fitted hyperbolic tangent model, the extraction of the inflection point denoting the boundary layer height from the fitted hyperbolic tangent model, and the consecutive percent reductions in the hydrogen ion concentration (Jorgensen and Revsbech 1985; Nishihara and Ackerman 2007; Hurd et al. 2011). For all profiles, there was an initial rapid decrease in pH followed by a linear decrease throughout the boundary layer before coalescing to bulk pH values, approximating a hyperbolic tangent function. To aid in the analysis and improve the fit of the hyperbolic tangent model, the initial pH values > 8.5 were omitted for all four boundary layer height protocols. The 99% method and the two hyperbolic tangent methods were in close agreement with each other and could discern differences across the profiles. The consecutive percent reduction method, on the other hand, was on average 1 cm less than the other methods and could not differentiate between profiles illustrated in its near uniform assessment of boundary layer heights (Figure S2). When the percentage threshold (ƒ), 10%, or consecutive count, n=4, was altered from the recommendations of Hurd *et al.* (2011), the boundary layer heights increased, but the variance was too high to discern differences between profiles or could not determine the boundary layer height (Figure S3). Further, the boundary layer heights from the 99% method and the hyperbolic tangent data intersection method were limited to the discrete sampling locations of the microsensor protocol. As such, the values locked in on discrete integer heights and had artificially low variances (Figure S2). Consequently, the fitted hyperbolic tangent model's boundary layer height was used for all analysis in the manuscript.

Supplementary Figures

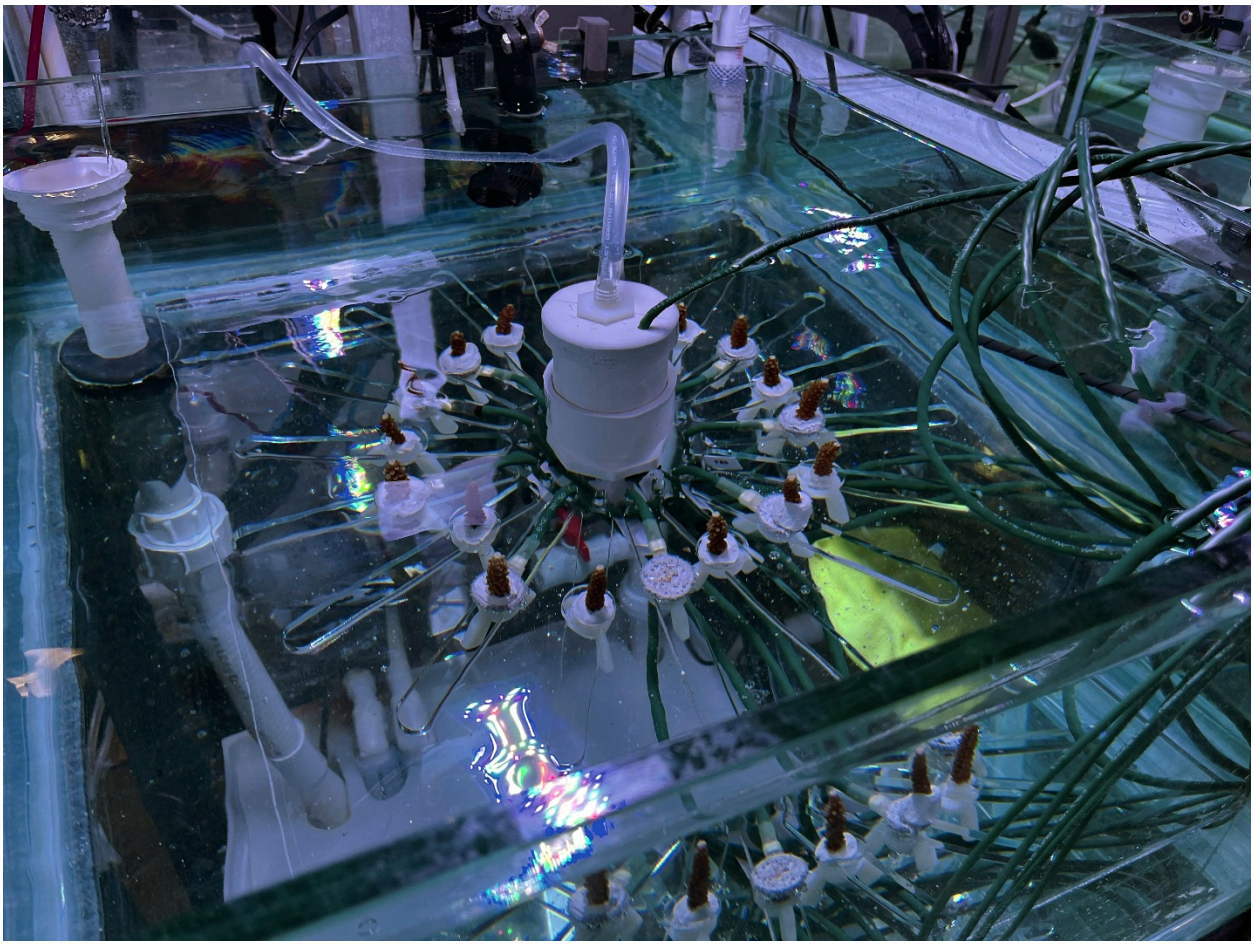

Figure S1 Assembled eAE system in the Experimental Reef Ecology Laboratory, University of Miami.

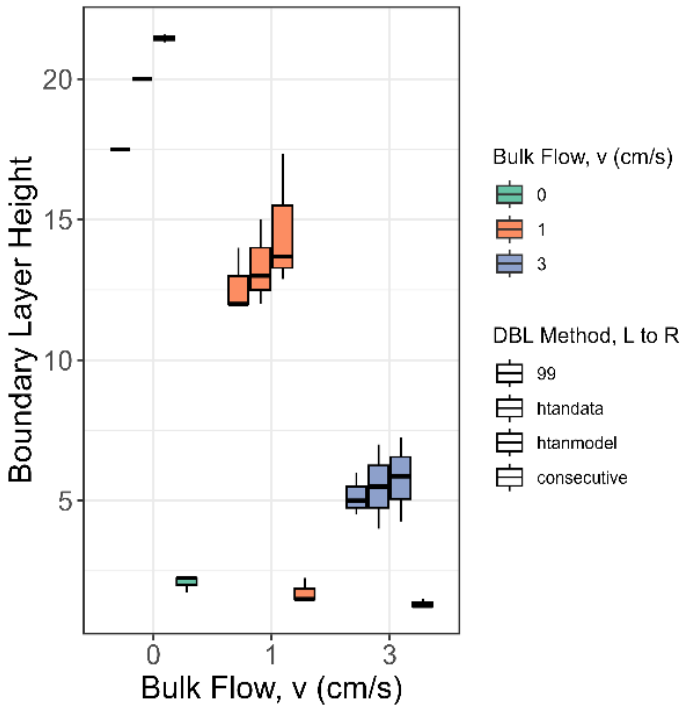

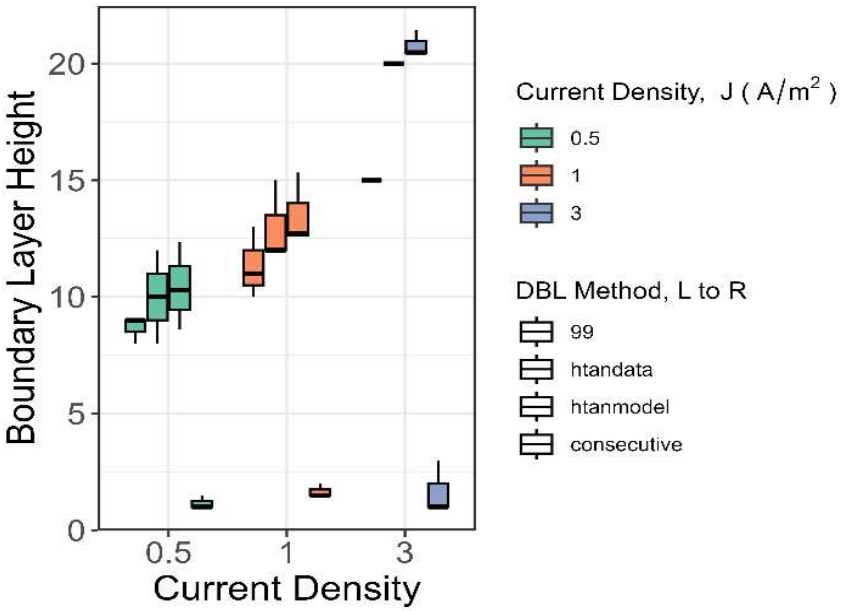

Figure S2 Alternative methods to determine the boundary layer height revealed peak-locking and low discernability that precluded their usefulness. From left to right, the methods are the intersection of the profile with 99% of its bulk concentration (99), the intersection of the profile with its fitted hyperbolic tangent model (htandata), the extraction of the inflection point denoting the boundary layer height from the fitted hyperbolic tangent model (htanmodel), and the consecutive percent reductions method (consecutive).

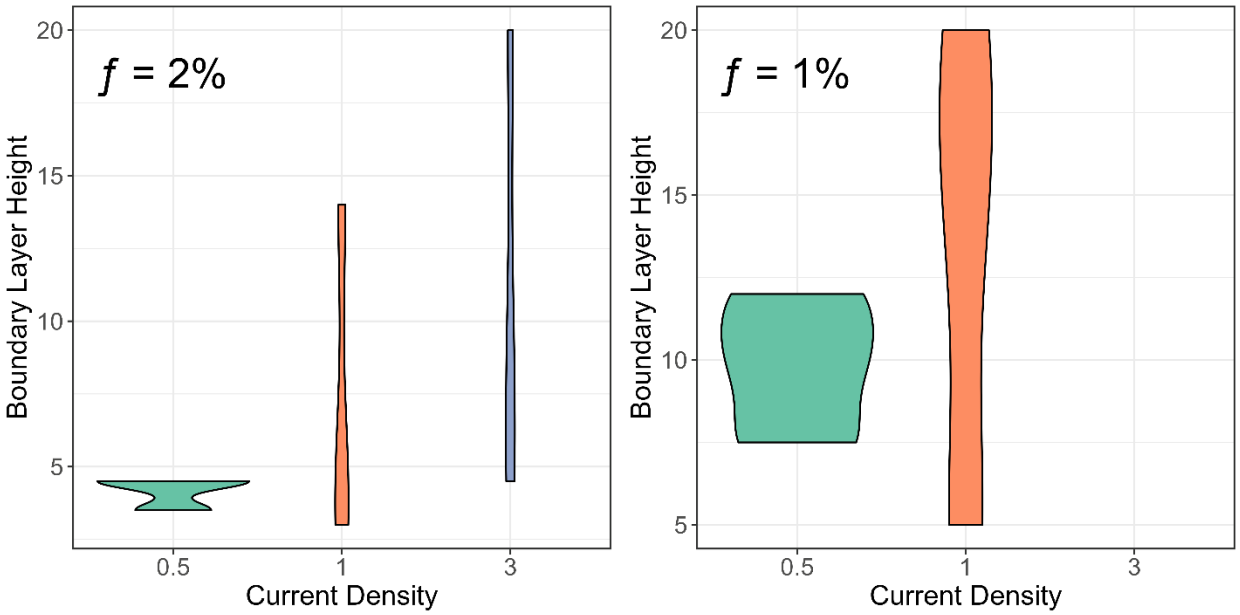

Figure S3 Decreasing the percentage threshold (ƒ) below the 10% recommendation from Hurd *et al.* (2011) increased the variance of the calculated boundary layer height.

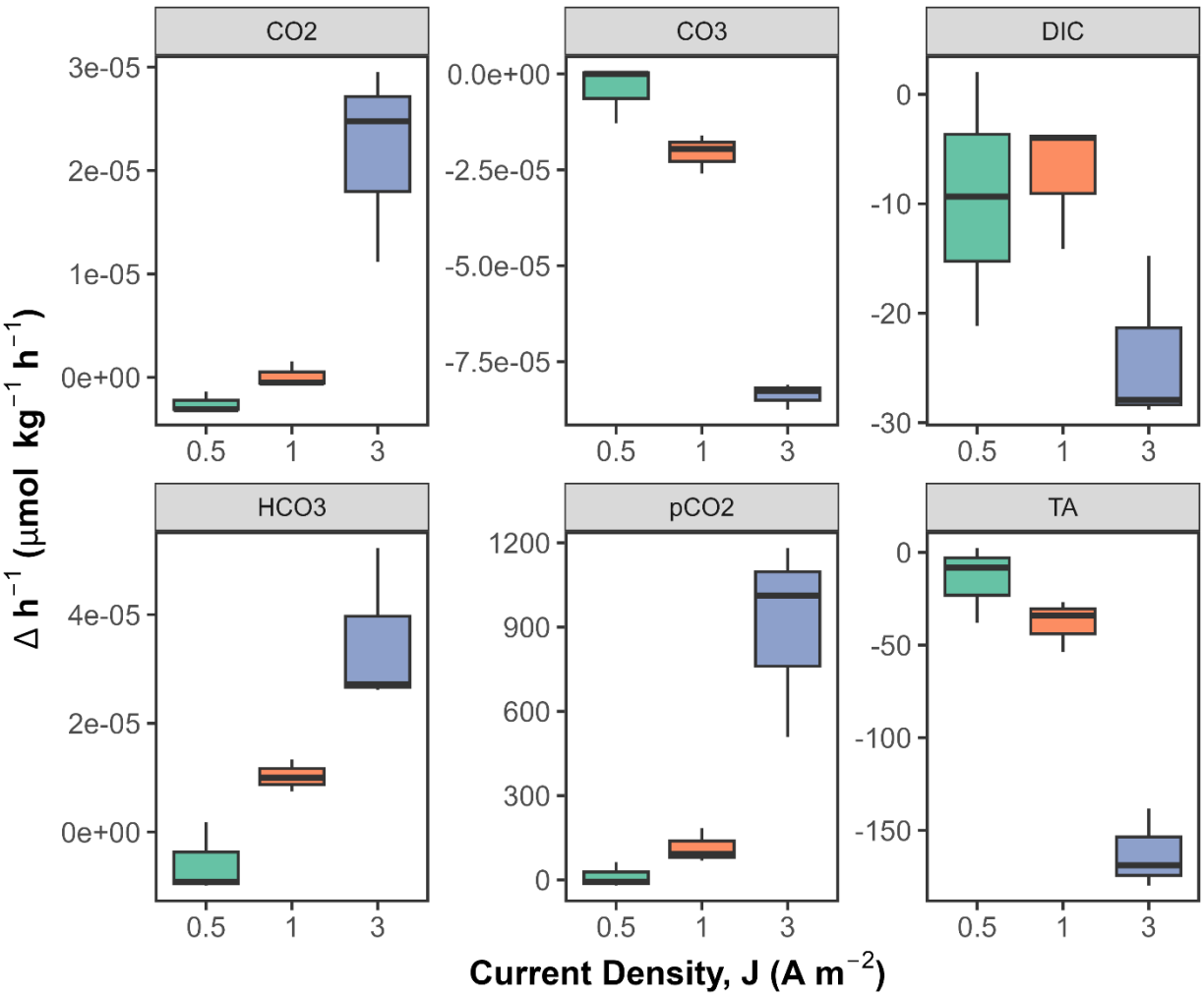

Figure S4. eAE carbonate chemistry incubations altered carbonate chemistry with increasing current density (A m^{-2}). The observed shifts reflect the combined effects of abiotic precipitation at the cathode and oxidative reactions at the anode, highlighting the influence of electrochemical processes on the seawater carbonate system in a closed system.

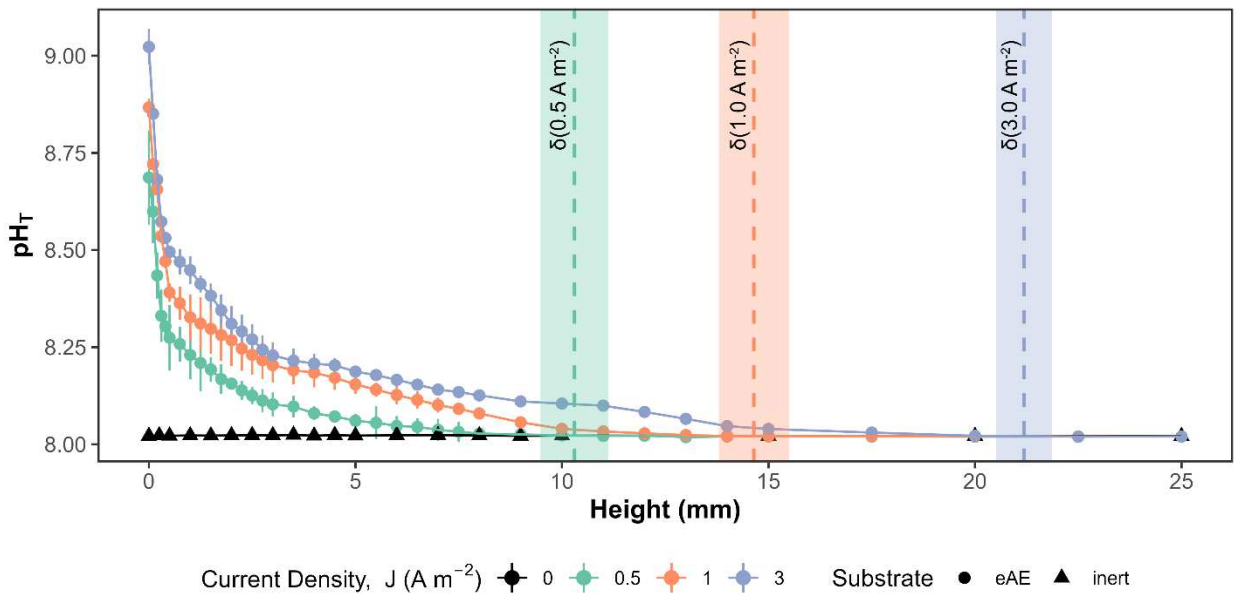

Figure S5. pH microsensor profiles above eAE (circles) and inert acrylic pucks (triangles) at three distinct electrical current densities (J, A m^{-2}), each measured with a flow speed of 1 cm s^{-1}. Vertical line segments centered on each point indicate ± 1 SD about the mean. Vertical dashed lines with surrounding ribbons represent the mean ± 1 SD of the boundary layer heights (δ) derived from the hyperbolic tangent model for each flow speed.

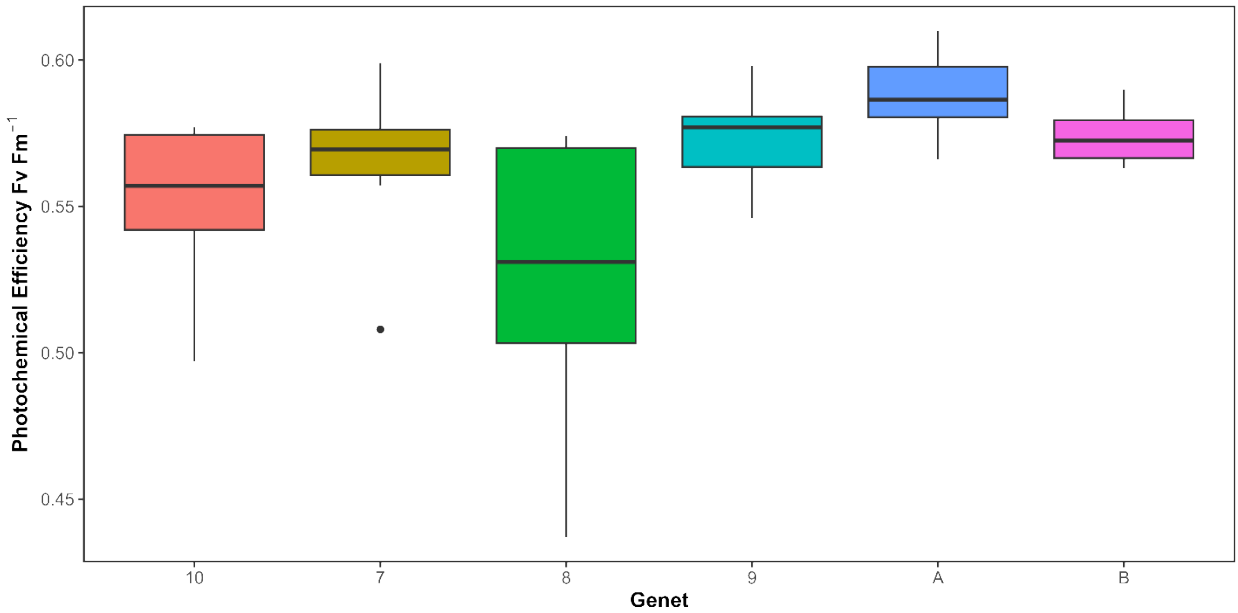

Figure S6. Genet-specific photochemical efficiency (Fv/Fm) highlight differences in photophysiology among genets at the conclusion of the experiment.

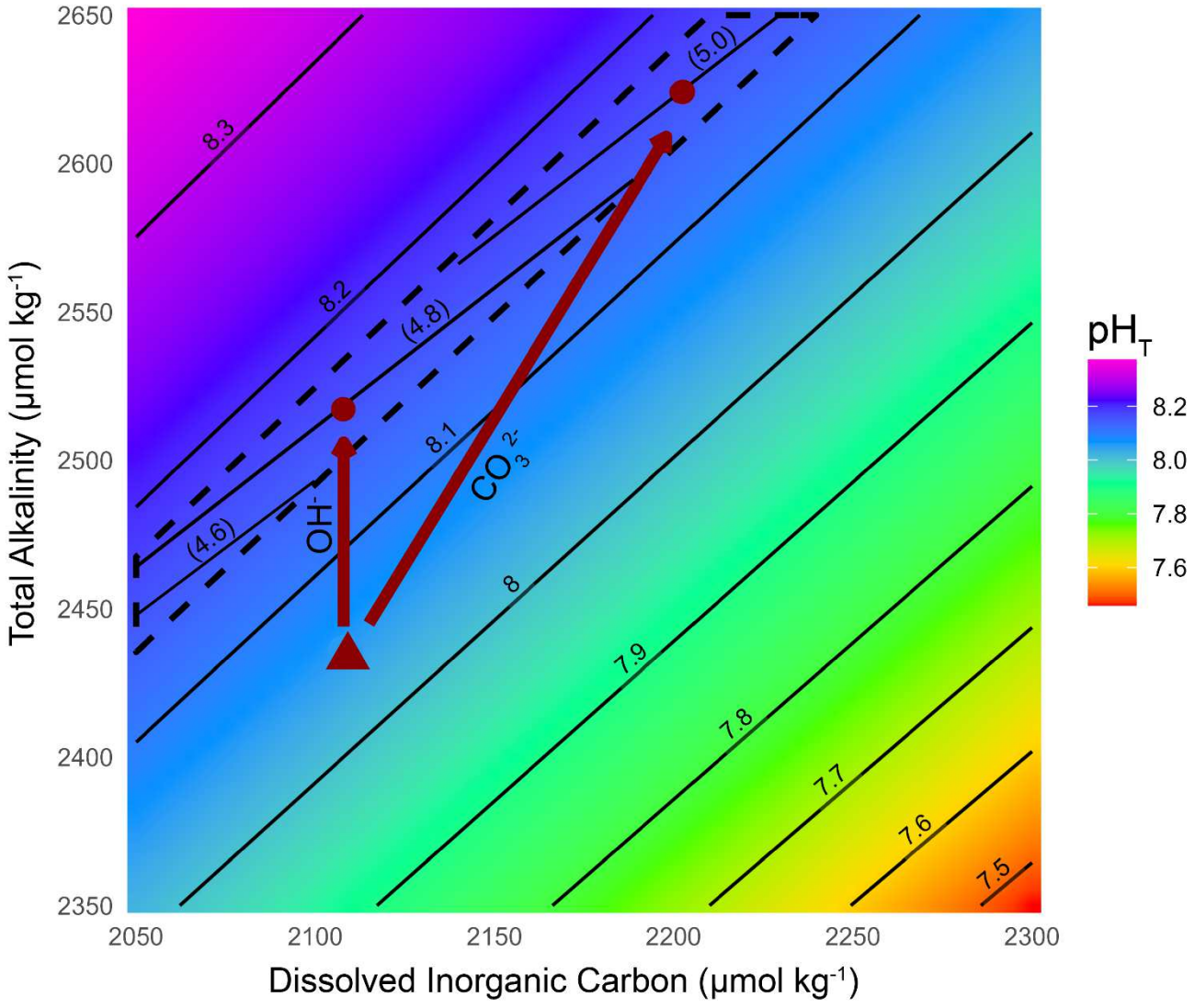

Figure S7. Carbonate chemistry property-property plot depicting the enhancement of the bulk water (triangle) to microenvironment carbonate chemistries (circles) with the electrochemical water reduction reaction (OH^-) and direct carbonate ion addition (CO_3^{2-}). Modeled water reduction reaction increased aragonite saturation states (Ω_{Ar}) from its initial value of 3.85 to 4.68, concomitant with a pH_T enhancement from 8.02 to 8.16. This contrasts with direct CO_3^{2-} addition, which would yield an Ω_{Ar} of 4.99 with the same pH_T of 8.16. Contour lines depict pH_T isopleths; parenthetically defined contour lines depict Ω_{Ar} within the dashed isopleth surrounding a pH_T of 8.16 ± 0.02. Arrows indicate the ionic additions required to raise the microenvironment pH_T with the respective ion.

Table S1. ANOVA model outputs for the effect of electrical current density (J) on carbonate chemistry parameters; degrees of freedom (df), sum of squares (SS), mean square (MS)

Term	*Fixed Effect*	*df*	*SS*	*MS*	*F*	*p-value*
TA	J	2	37763	18881	51.9	1.63e-4
DIC	J	2	485.0	242.52	3.136	0.117
pCO2	J	2	1417859	708929	16.61	3.58e-3
CO2	J	2	1.069e-09	5.347e-10	17.17	3.29e-3
HCO3	J	2	2.553e-09	1.276e-09	14.16	5.34e-3
CO3	J	2	1.06e-08	5.299e-09	169.2	5.28e-06

Table S2 Average pH_T at heights (mm) above the cathode as a function of flow speed (cm s^{-1}) and current density (A m^{-2}) data, see vertical dashed lines in Figure 2**.**

Flow speed (cm s^{-1})	**Current density (A m^{-2})**	**Height (mm)**	**pH_T**	**SD**	**N**
0	1	5	8.218	0.008	3
0	1	15	8.052	0.001	3
1	0.5	5	8.061	0.006	3
1	0.5	15	8.020	0.001	3
1	1	5	8.160	0.022	6
1	1	15	8.022	0.002	6
1	3	5	8.187	0.013	3
1	3	15	8.040	0.001	3

3	1	5	8.035	0.013	3
3	1	15	8.020	0.000	3

Table S3. ANOVA model outputs for the effect of flow speed (v) and electrical current density (J) on pH boundary layer heights; degrees of freedom (df), sum of squares (SS), mean square (MS)

Term	*Fixed Effect*	*df*	*SS*	*MS*	*F*	*p-value*
Boundary layer	J	2	180143675	90071838	145.6	8.23e-6
pH-0mm	J	2	0.16982	0.08491	59.99	1.08e-4
pH-5mm	J	2	0.25858	0.012929	50.76	1.74e-4
pH-15mm	J	2	7.02e-04	3.51e-04	139.2	9.38e-6
Boundary layer	V	2	360885100	180442550	100.5	2.44e-5
pH-0mm	v	2	0.0000816	0.0000408	0.091	0.915
pH-5mm	v	2	0.05338	0.026688	100.9	2.41e-5
pH-15mm	v	2	0.0019677	0.0009838	358.3	5.72e-7

Table S4. Linear mixed effects model output for the effect of eAE and inert substrates on the calcification rates of *A. cervicornis*; standard error (se), degrees of freedom (df).

Fixed Effect	*Estimate*	*df*	*se*	*t-value*	*p-value*
substrate	-0.05197	59.76384	0.039	-1.348	0.183

Table S5. Generalized linear mixed-effects model output for the effect of growth experiments on the carbonate chemistry system; standard error (se), degrees of freedom (df).

Fixed Effect	*estimate*	*se*	*t-value*	*p-value*
experiment	-0.212	0.017	-12.365	4.04E-35
CO3	2.882	0.016	185.311	0.00E+00
DIC	5.125	0.016	329.478	0.00E+00
HCO3	5.006	0.016	321.830	0.00E+00
Omega	-1.242	0.016	-79.860	0.00E+00
pCO2	3.634	0.016	233.662	0.00E+00

salinity	1.006	0.016	64.674	0.00E+00
spectrophotometric pH	-0.451	0.016	-29.006	5.48E-185
TA	5.260	0.016	338.203	0.00E+00
Temperature	0.799	0.016	51.400	0.00E+00
experiment:CO3	0.362	0.024	14.946	1.65E-50
experiment:DIC	0.205	0.024	8.459	2.71E-17
experiment:HCO3	0.186	0.024	7.662	1.83E-14
experiment:Omega	0.368	0.024	15.173	5.35E-52
experiment:pCO2	-0.008	0.024	-0.345	7.30E-01
experiment:salinity	0.185	0.024	7.652	1.98E-14
experiment:spectrophotometric pH	0.223	0.024	9.216	3.10E-20
experiment:TA	0.227	0.024	9.362	7.84E-21
experiment:Temperature	0.207	0.024	8.538	1.37E-17

Table S6. Linear mixed effects model output for the effect of eAE and inert substrates, fragment height, and their interaction on the calcification rates of *P. clivosa*; standard error (se), degrees of freedom (df).

Fixed Effect	*Estimate*	*se*	*df*	*t-value*	*p-value*
Substrate	-0.223	0.044	4.952	-5.020	4.14e-3
Height	-0.181	0.038	42.299	04.738	2.45e-5
Substrate:Height	0.201	0.054	41.987	3.740	5.52e-4

Table S7. Linear mixed effects model output for the effect of experiment on the abiotic mineral precipitation bulk mass change rates; standard error (se), degrees of freedom (df).

Fixed effect	*Estimate*	*se*	*df*	*t-value*	*p-value*
experiment	-8.218	5.037	10.791	-1.632	0.132

Table S8. Linear mixed-effects model output for the effect of substrate, height, and their interaction on planar areas. Fixed effects each interact with time to calculate planar tissue growth rates (cm^{-2} day^{-1}); standard error (se), degrees of freedom (df).

Fixed Effect	*Estimate*	*se*	*df*	*t-value*	*p-value*
Days	0.032	0.002	136.8	19.020	<2e-16
Days:substrate	-0.011	0.002	136.4	-4.500	1.44e-05
Days:height	-0.013	0.002	136.7	-5.447	2.31e-07
Days:substrate:height	0.010	0.003	136.4	2.976	0.00346

Table S9. Linear mixed-effects model output for the effect of substrate and height on photochemical efficiency values (Fv/Fm).

Fixed Effect	*Estimate*	*SE*	*df*	*T value*	*P value*
substrate	-0.018	2.20e-2	2.46	-0.827	0.481
height	0.000	1.0e-2	37.0	0.070	0.945
substrate:height	-0.009	1.35e-2	37.0	-0.634	0.530

Table S10. ANOVA model outputs for the effect of genet on photochemical efficiency values (Fv/Fm); degrees of freedom (df), sum of squares (SS), mean square (MS)

Term	*Fixed Effect*	*df*	*SS*	*MS*	*F*	*p-value*
Fv/Fm	genet	5	2.10e-2	4.20e-3	4.82	1.44e-3

Supplementary Files

This is a list of supplementary files associated with this preprint. Click to download.

- kiel2025eAESupplementaryMaterials.docx